Propagation Effects of Slanted Narrow Bipolar Events: A Rebounding-Wave Model Study

Dongshuai Li[1], Alejandro Luque[2], Farhad Rachidi[3], Marcos Rubinstein[4], Torsten Neubert[5], Yanan Zhu[6], Olivier Chanrion[7], Caitano da Silva[8], and Paul Krehbiel[8]

[1]National Space Institute, Technical University of Denmark (DTU Space)
[2]Institute for Astrophysics of Andalusia (IAA-CSIC), in Granada, Spain
[3]Swiss Federal Institute of Technology (EPFL)
[4]University of Applied Sciences of Western Switzerland
[5]Department of Solar System Physics, Denmark
[6]Earth Networks
[7]National Space Institute (DTU Space)
[8]New Mexico Tech

September 11, 2023

Abstract

Narrow bipolar events (NBEs) are impulsive and powerful intracloud discharges. Recent observations indicate that some NBEs exhibit a slanted orientation rather than strictly vertical. However, the inclination of NBEs has not been considered in previous transmission line models, leading to uncertainty when evaluating their characteristics based on electromagnetic fields. This paper investigates the propagation effects of slanted NBEs using a newly developed slanted rebounding-wave model. It is found that the calculated results using the proposed model match well with measurements for both vertical and slanted NBE cases. The inclination of the NBEs significantly affects the electromagnetic fields at close distances, while the effects weaken as the observation distance increases, where the fields are dominated by the radiation component. The slanted rebounding-wave model improves the agreement with respect to a purely vertical channel and can be extended to any discharge geometry at arbitrary observation distances.

Propagation Effects of Slanted Narrow Bipolar Events: A Rebounding-Wave Model Study

Dongshuai Li[1,2], Alejandro Luque[2], Farhad Rachidi[3], Marcos Rubinstein[4], Torsten Neubert[1], Yanan Zhu[5], Olivier Chanrion[1], Caitano da Silva[6], Paul R. Krehbiel[6]

[1]National Space Institute, Technical University of Denmark (DTU Space), Kongens Lyngby, Denmark.
[2]Instituto de Astrofísica de Andalucía (IAA), CSIC, Granada, Spain.
[3]Electromagnetic Compatibility Laboratory, Swiss Federal Institute of Technology (EPFL), Lausanne, Switzerland.
[4]University of Applied Sciences and Arts Western Switzerland, Yverdon-les-Bains, Switzerland.
[5]Earth Networks, Germantown, Maryland, USA.
[6]Langmuir Laboratory for Atmospheric Research, New Mexico Institute of Mining and Technology, Socorro, USA.

Key Points:

- The propagation effect of slanted NBEs at different distance is investigated and compared with the observations.
- The inclination of the NBEs could significantly affect the electromagnetic fields in the close distance.
- The proposed equations will improve the quality of inferred features of slanted NBEs and can be extended to any discharge shape.

Corresponding author: Dongshuai Li[1,2] and Alejandro Luque[2],

[1] National Space Institute, Technical University of Denmark (DTU Space), Kongens Lyngby, Denmark.
[2] Instituto de Astrofísica de Andalucía (IAA), CSIC, Granada, Spain., (dongshuai@space.dtu.dk, aluque@iaa.es)

Abstract

Narrow bipolar events (NBEs) are impulsive and powerful intracloud discharges. Recent observations indicate that some NBEs exhibit a slanted orientation rather than strictly vertical. However, the inclination of NBEs has not been considered in previous transmission line models, leading to uncertainty when evaluating their characteristics based on electromagnetic fields. This paper investigates the propagation effects of slanted NBEs using a newly developed slanted rebounding-wave model. It is found that the calculated results using the proposed model match well with measurements for both vertical and slanted NBE cases. The inclination of the NBEs significantly affects the electromagnetic fields at close distances, while the effects weaken as the observation distance increases, where the fields are dominated by the radiation component. The slanted rebounding-wave model improves the agreement with respect to a purely vertical channel and can be extended to any discharge geometry at arbitrary observation distances.

Plain Language Summary

Narrow Bipolar Events (NBEs) are unique intracloud discharges that occur either individually or as the initiation event for lightning flashes inside thunderstorms. Knowing the physical mechanisms of NBEs will help us to better understand how lightning initiates inside thunderstorms. Recent studies indicated that NBEs could exhibit a slanted orientation rather than being strictly vertical. Here, in the light of these observations, we analyze the propagation effect of the slanted NBEs by using a newly developed slanted rebounding-wave model, and we compare the modeling results with observations. This study contributes to a better understanding of the physical mechanism of NBEs and provides a reference for accurately characterizing NBEs based on their electromagnetic fields.

1 introduction

In recent years, significant attention has been given to Narrow Bipolar Events (NBEs) due to their important role in lightning initiation (Rison et al., 2016; Tilles et al., 2019; Lyu et al., 2019). NBEs are generated by the intracloud discharges that emit strong radiation in the high and very high frequency (HF/VHF) range (Le Vine, 1980; Smith et al., 1999, 2004), and they are characterized by fast breakdowns (FBs) that appear to be a system of streamer coronas (Rison et al., 2016; Phelps, 1974; Phelps & Griffiths, 1976; Attanasio et al., 2021; Tilles et al., 2019; Lyu et al., 2019; Attanasio et al., 2019). However, the exact physical mechanism behind NBEs still remains unclear.

The transmission line model is widely recognized as the most commonly used approach for inferring the characteristics of NBEs based on their electromagnetic fields. NBEs typically have channel lengths ranging from hundreds of meters to a few kilometers (Smith et al., 1999, 2004). When observing NBEs at distances as large as hundreds of kilometers, only the radiation field component is observable. Therefore, many studies simplify the NBE channel by assuming it to be an infinitesimally short dipole (Smith et al., 1999, 2004; Eack, 2004). This has led to misinterpretation of electric current intensities in all types of pulses taking place during the initial breakdown stage of lightning, as discussed by da Silva et al. (2016b). However, for close-range observations within a few kilometers or less, where induction and electrostatic fields are also significant, more accurate transmission line-based models of NBEs are proposed in the literature. These models include the classic transmission line (TL) model (Watson & Marshall, 2007), the modified transmission line with exponential increase (MTLEI) model (Watson & Marshall, 2007), the bouncing-wave transmission line model (Nag & Rakov, 2010), the modified transmission line with exponential decay (MTLE) model (Rison et al., 2016; Karunarathne et al., 2016) and the modified transmission line-gaussian (MTLG) model (da Silva et al., 2016a; R. A. Marshall et al., 2015). Attanasio et al. (2021) argued that, from an electrostatic standpoint, the precursor streamer system can produce a strong electric field enhancement ahead of itself that may trigger a rebounding opposite-polarity event traveling back towards the origin. Recently, Li, Luque, Gordillo-Vázquez, et al. (2022) introduced a rebounding-wave model based on the Modified Transmission Line with Exponential decay (MTLE) model (Nucci & Rachidi, 1989; Rachidi & Nucci, 1990; Rison et al., 2016), termed “rebounding MTLE model”, to represent the subsequent streamer features involved in NBEs (Rison et al., 2016;

Tilles et al., 2019; Attanasio et al., 2021). A common feature of all the transmission line-based models is the assumption that the NBE channel is vertically oriented.

Recent observations indicate that NBEs could be tilted from vertical and exhibit a noticeable spread in azimuthal values (Rison et al., 2016). Karunarathne et al. (2016) estimated the three-dimensional charge moments of ten NBEs and found that three of them were tilted at angles ranging from 10 to 20 degrees from the vertical. R. A. Marshall et al. (2015) suggested that slanted NBEs play a role in the illumination of the lower ionosphere known as "elve doublets". Particularly, these authors suggested that if the NBE source current is inclined towards the observer, the second elve in the doublet can be brighter than the first. However, the impact of channel inclination on the propagation effects of NBEs at different distances remains unknown. Here, following previous studies on the effect of the inclination and tortuosity of lightning return stroke channels (Le Vine & Meneghini, 1978b,a; Abouzeid & Zein El Dein, 2015), we propose an extension of the rebounding wave model of Li, Luque, Gordillo-Vázquez, et al. (2022) for NBEs. The so-called slanted rebounding wave model is firstly validated against a full-wave three-dimensional Finite-Difference Time-Domain (FDTD) method and then through comparisons with observations reported in the literature.

2 Slanted rebounding wave model

The slanted transmission line model was firstly proposed by Abouzeid & Zein El Dein (2015) to analyze the effect of lightning return stroke channel tortuosity and branching. In this study, we extend their equations to investigate the inclination of the NBE channel. NBE is considered as a system of streamer coronas represented by the a rebounding-wave model based on the Modified Transmission Line with Exponential decay (MTLE) (Nucci & Rachidi, 1989; Rachidi & Nucci, 1990; Rison et al., 2016), termed "rebounding MTLE model" (Li, Luque, Gordillo-Vázquez, et al., 2022).

As illustrated in Figure 1, the positive streamer coronas propagate downwards from an altitude H_2 to an altitude H_1 with a channel length L (for a slanted channel $H_1 = H_2 - r\cos\theta$), followed by upward negative streamer corona discharges that propagate back along the same path. I_d is the downward current (red color) and I_u is the rebounding-wave current (blue color). According to the rebounding MTLE model (Li, Luque, Gordillo-Vázquez, et al., 2022), the total current $I(r,t)$ is the sum of the downward current $I_d(r,t)$ and the upward rebounding current $I_u(r,t)$. Both currents are assumed to experience an exponential decay along the same propagation channel with attenuation rates of λ_d and λ_u, respectively. The total current and the downward and upward rebounding currents are given by

$$\begin{aligned} I(r,t) &= I_d(r,t) + I_u(r,t), \\ I_d(r,t) &= I(t-(L-r)/v_d)e^{-(L-r)/\lambda_d}, \\ I_u(r,t) &= I(t-L/v_d - r/v_u)e^{-L/\lambda_d}e^{-r/\lambda_u}, \end{aligned} \tag{1}$$

where v_d and v_u are the downward and upward propagation velocities. The factor e^{-L/λ_d} ensures the continuity between the downward and the upward-propagating currents.

In free space, the vertical electric field E_z at the observation point $P(x_p, y_p, z_p)$, where $x_p = \rho\cos(\phi_p)$ and $y_p = \rho\sin(\phi_p)$, due to a short inclined dipole dr carrying the current $I(r,t)$ located at a height $(H_2 - r\cos\theta)$ is given as:.

$$
\begin{aligned}
dE_{zc} = & \frac{dr}{4\pi\epsilon_0} \\
& \begin{pmatrix}
\begin{pmatrix}
\frac{3(z_p-(H_2-r\cos\theta))(x_p-r\sin\theta\cos\phi)}{R^5(r)}\sin\theta\cos\phi \\
+\frac{3(z_p-(H_2-r\cos\theta))(y_p-r\sin\theta\sin\phi)}{R^5(r)}\sin\theta\sin\phi \\
+\frac{3(z_p-(H_2-r\cos\theta))^2-R^2(r)}{R^5(r)}\cos\theta
\end{pmatrix} \int_0^t I(r,t)d\tau \\
\begin{pmatrix}
\frac{3(z_p-(H_2-r\cos\theta))(x_p-r\sin\theta\cos\phi)}{cR^4(r)}\sin\theta\cos\phi \\
+\frac{3(z_p-(H_2-r\cos\theta))(y_p-r\sin\theta\sin\phi)}{cR^4(r)}\sin\theta\sin\phi \\
+\frac{3(z_p-(H_2-r\cos\theta))^2-R^2(r)}{cR^4(r)}\cos\theta
\end{pmatrix} I(r,t) \\
\begin{pmatrix}
\frac{(z_p-(H_2-r\cos\theta))(x_p-r\sin\theta\cos\phi)}{c^2R^3(r)}\sin\theta\cos\phi \\
+\frac{(z_p-(H_2-r\cos\theta))(y_p-r\sin\theta\sin\phi)}{c^2R^3(r)}\sin\theta\sin\phi \\
+\frac{(z_p-(H_2-r\cos\theta))^2-R^2(r)}{c^2R^3(r)}\cos\theta
\end{pmatrix} \frac{\partial I(r,t)}{\partial t}
\end{pmatrix},
\end{aligned}
\tag{2}
$$

where,

$$
R(r) = \sqrt{(x_p - r\sin\theta\cos\phi)^2 + (y_p - r\sin\theta\sin\phi)^2 + (z_p - (H_2 - r\cos\theta))^2}. \tag{3}
$$

Individual terms on the right hand side of Equation (2) containing the factors are the electrostatic, induction and radiation components. If we assume the ground as a perfectly conducting plane, its effect can be taken into account using image theory, yielding

$$
\begin{aligned}
dE_{zm} = & -\frac{dr}{4\pi\epsilon_0} \\
& \begin{pmatrix}
\begin{pmatrix}
\frac{3(z_p+(H_2-r\cos\theta))(x_p-r\sin\theta\cos\phi)}{R_0^5(r)}\sin\theta\cos\phi \\
+\frac{3(z_p+(H_2-r\cos\theta))(y_p-r\sin\theta\sin\phi)}{R_0^5(r)}\sin\theta\sin\phi \\
-\frac{3(z_p+(H_2-r\cos\theta))^2-R_0^2(r)}{R_0^5(r)}\cos\theta
\end{pmatrix} \int_0^t I(r,t)d\tau \\
\begin{pmatrix}
\frac{3(z_p+(H_2-r\cos\theta))(x_p-r\sin\theta\cos\phi)}{cR_0^4(r)}\sin\theta\cos\phi \\
+\frac{3(z_p+(H_2-r\cos\theta))(y_p-r\sin\theta\sin\phi)}{cR_0^4(r)}\sin\theta\sin\phi \\
-\frac{3(z_p+(H_2-r\cos\theta))^2-R_0^2(r)}{cR^4(r)}\cos\theta
\end{pmatrix} I(r,t) \\
\begin{pmatrix}
\frac{(z_p+(H_2-r\cos\theta))(x_p-r\sin\theta\cos\phi)}{c^2R_0^3(r)}\sin\theta\cos\phi \\
+\frac{(z_p+(H_2-r\cos\theta))(y_p-r\sin\theta\sin\phi)}{c^2R_0^3(r)}\sin\theta\sin\phi \\
-\frac{(z_p+(H_2-r\cos\theta))^2-R_0^2(r)}{c^2R^3(r)}\cos\theta
\end{pmatrix} \frac{\partial I(r,t)}{\partial t}
\end{pmatrix},
\end{aligned}
\tag{4}
$$

where,

$$
R_0(r) = \sqrt{(x_p - r\sin\theta\cos\phi)^2 + (y_p - r\sin\theta\sin\phi)^2 + (z_p + (H_2 - r\cos\theta))^2}. \tag{5}
$$

For an observer P located on the ground surface, the height of the observation point z_p is equal to zero in all the equations above, implying $R = R_0$. The total vertical electric field E_z for the whole inclined channel can be obtained by integrating the dipole field dE_{zc} and its image dE_{zm} over the entire channel. Note that both the dipole field dE_{zc} and its image dE_{zm} include the slanted feature of the sources, and they reduce to the case of a vertical channel when the polar angle $\theta = 0$ (Thottappillil & Rakov, 2001; M. A. Uman et al., 1975). Moreover, the equations are not limited to straight channel but also can be applied to any arbitrarily tortuous discharge channel by approximating it as a series of small straight segments.

Although not mentioned in the study of Abouzeid & Zein El Dein (2015), the so-called discontinuity term (Thottappillil et al., 1998; Thottappillil & Rakov, 2001),"turn-on" term (M. A. Uman & McLain, 1970; M. A. Uman Martin A. & McLain, 1970) or F factor (Rubinstein & Uman, 1990; Thottappillil & Rakov, 2001, 2005; Shao et al., 2004, 2005) should be considered if there is a current discontinuity at the propagation wave front. The equations for the discontinuity term are given in Text S1 in Supporting Information.

3 Validation of the slanted rebounding wave model

To validate the proposed slanted transmission line equations for NBEs, we compare its prediction against a full-wave three-dimensional FDTD model (Li et al., 2016, 2017). In the simulation, the NBE source is assumed to be a dipole at an altitude $H = 5\,\mathrm{km}$ above a perfectly conducting ground with different polar angle θ of 0°, 30°, 60° and 90°. The current waveform is given by double-exponential expression with $I(t) = I_0(e^{\alpha t}/(1 + e^{(\alpha+\beta)t})$, where the rise time constant is $\alpha = 1/\tau_1$ and the fall time constant is $\beta = 1/\tau_2$ (Rison et al., 2016). The values of τ_1 and τ_2 are 1 µs and 5 µs, respectively. The peak current is normalized to $I_{peak} = -100\,\mathrm{kA}$ by setting $I_0 = I_{peak}(1 + \frac{\alpha}{\beta})(\frac{\alpha}{\beta})^{(\frac{-\alpha}{\alpha+\beta})}$.

For a vertical dipole with $\theta = 0°$, the electric field varies with azimuthal symmetry, but it is more complicated for the slanted cases showing different features depending on the different azimuthal angles. The comparison between the slanted rebounding wave model and the FDTD method for both vertical and slanted dipoles is given in Figure 2. The results calculated by the presented equations match perfectly with the FDTD results for both vertical and slanted sources. For horizontal dipole with $\theta = 90°$, the electric field first increases within a distance of 5 km and then decreases as the observer moves away from the source and becomes negligible beyond a distance of about 50 km.

The results from the FDTD simulation are further shown in Figure S1 and S2 in Supporting Information. Figure S1 shows the side view (a, c, e, g) and top view (b, d, f, h) of a snapshot of the FDTD simulation for the vertical electric fields of the slanted dipole with $\theta = 0°$, 30°, 60° and 90°. Figure S2 illustrates the electrostatic, induction and radiation components for both vertical and slanted dipoles at different distances. The inclination of the source at closer distances ($\leq$ 10 km) causes a significant effect on the electrostatic and induction components of the electric fields. Both the waveshape and the amplitude of the electric field are influenced by the inclination of the source (see Figure S2(d1, d2, d3)). In our case, the reversal distance (Nag & Rakov, 2010), where the electrostatic and induction components of the field reverse their polarity, varies as a function of the slanted dipole angle. As shown in Figure S2(d2, e2, d3 and e3), the tail part of the waveform becomes higher due to the increase of the electrostatic fields caused by the slant angle. For distances beyond 50 km, the electric field is dominated by the radiation component, and the inclination only affects the amplitudes (see Figure S2(d4 and e4)). It is interesting to note that the effect of the slant angle lower than 30° becomes weak beyond a distance of about 10 km. However, the effect of slant angles bigger than 30° could not be ignored even at distances as large as 50 km.

4 Comparison with the observations in the literature

4.1 The electrical discharges following NBEs

Recent studies reported that the electric fields of NBEs at distances below 10 km include two parts: a main bipolar pulse characteristic of NBE and a slow electrostatic change lasting from tens of microseconds to a few milliseconds (Karunarathne et al., 2016; T. Marshall et al., 2014). The slow electrostatic change following NBEs seems to be related to the attempted electrical activities that never developed into a full lightning flash (Karunarathne et al., 2016). This fact is also supported by the multi-pulse corona discharges observed by the Atmosphere-Space Interactions Monitor (ASIM) onboard International Space Station (ISS) (Li, Luque, Lehtinen, et al., 2022; Li et al., 2023). In their study, Li, Luque, Lehtinen, et al. (2022) found that, for the multi-pulse corona discharges, the first optical pulse coincides with a strong radio signal in the form of a NBE but subsequent optical pulses, delayed by some milliseconds, are related to horizontally oriented streamer-like electrical discharges which do not trigger full-fledged lightning. However, it remains unclear whether these electrical discharges following NBEs are part of the NBEs produced by the remaining streamer corona activities (Rison et al., 2016; Li, Luque, Gordillo-Vázquez, et al., 2022) or if they are independent electrical discharges, similar to the Initial E-Change (IEC) that occurs before the first initial breakdown pulses of a lightning flash (T. Marshall et al., 2014, 2019; Kostinskiy et al., 2020).

In our study, we consider these electrical discharges as an extra long decay current I_{extra} along with the main NBE current, despite lacking knowledge about their physical mechanism. The current is represented using the double-exponential expressions (Rison et al., 2016),

$$I(t) = I_{NBE}(t) + I_{extra}(t) = I_0 \frac{e^{\alpha t}}{1 + e^{(\alpha+\beta)t}} + \eta I_0 \frac{e^{\alpha t}}{1 + e^{(\alpha+\gamma)t}}, \tag{6}$$

where the rise time constant for the original streamer current $\alpha = 1/\tau_1$ and the fall time constant for the original streamer current $\beta = 1/\tau_2$. For the extra current $\gamma = 1/\tau_3$. $0 \leq \eta \leq 1$ is the fraction of the extra current $I_{extra}(t)$ compared to the primary NBE current $I_{NBE}(t)$. The peak value of I_{NBE} is normalized to I_{peak} by setting $I_0 = I_{peak}(1 + \frac{\alpha}{\beta})(\frac{\alpha}{\beta})^{(\frac{-\alpha}{\alpha+\beta})}$.

4.2 Comparison with the observations reported by Rison et al. (2016)

In this section, we compare the simulated results obtained by the slanted rebounding wave model with the electric fields measured by a fast antenna (FA) for the vertical and slanted cases reported by Rison et al. (2016). According to interferometer (INTF) observations, the NBEs consisted of a downward Fast Positive Breakdown (FPB) followed immediately by an upward Fast Negative Breakdown (FNB) that propagated back in the opposite direction along the previous path. In the simulation, we model the fast breakdown of the NBE as a system of positive streamers that propagate downwards over a distance L, then upwards back along the previous path as predicted by the rebounding MTLE model (Li, Luque, Gordillo-Vázquez, et al., 2022). The same double-exponential current is adopted for the comparison with the results of Rison et al. (2016).

According to Equation (1), the total current $I(r,t)$ is the sum of the downward current $I_d(r,t)$ and the upward rebounding current $I_u(r,t)$, where $v_d = L/t_d$ and $v_u = L/t_u$ are the downward and upward velocities related to the inferred downward and upward propagation times t_d and t_u obtained by fitting the INTF traces for both NBE1 and NBE3 with the best fit lines shown in Li, Luque, Gordillo-Vázquez, et al. (2022) (see Figure 2 there).

As mentioned by Rison et al. (2016), the NBE1 discharge occurred at constant azimuth consistent with the positive breakdown being vertically downward (see Figure 7 in the Supplementary Material of Rison et al. (2016)). On the other hand, NBE3 showed substantial azimuthal spread with nonnegligible tilt from vertical (see Figure 9 in the Supplementary Material of Rison et al. (2016)). Firstly, we assume the channel to be vertical ($\theta = 0$) for both NBE1 and NBE3. Note that the results by assuming both NBE1 and NBE3 to be vertical are discussed in Li, Luque, Gordillo-Vázquez, et al. (2022). Here we also present the results in Figure 3 with the best-fit parameters listed in Table S1 in Supporting Information. The estimated charge moment change Q_{mom} for the vertical NBE1 and vertical NBE3 are $-215\,\mathrm{C\cdot m}$ and $-116\,\mathrm{C\cdot m}$, respectively. It is found that the simulated results for NBE1 agree well with the observations. However, this is not the case for the slanted case of NBE3, for which significant deviations can be observed, especially in the tail part of the waveform.

In order to investigate the effect of the inclination of NBE sources on the fields, we introduce an additional free parameter, the polar angle θ, to represent the effect of inclination. To simplify the geometry, we assume that the plane containing the NBE channel is perpendicular to the transfer vector from the INTF observations' geometry to the geometry used in Figure 1 (see Text S2 and Figure S3 in Supporting Information). The azimuth angle for the source $\phi = 249°$ and for the observation point P, $\phi_p = 160°$, are estimated based on the transformation. The simulated result for the slanted NBE3 is presented in Figure 3(c) with the inferred features shown in Table S1 in Supporting Information. By considering the simulation-estimated polar angle of $\theta = 15°$, the simulated waveform for NBE3 reasonably agrees with the measurement, corresponding to a charge moment change of $-357\,\mathrm{C}\cdot\mathrm{m}$, which is three times larger than the vertical case. However, the observed flattening tail part of NBE3 still could not be matched well. This suggests that NBE3 might involve more complicated processes than just being slanted.

As mentioned earlier, the electrostatic offset of NBE3 could be produced by the remaining streamer activities following NBEs (Rison et al., 2016). To address this, we introduce an additional long decay current, I_{extra}, derived from the presence of the remaining streamer corona activities of NBE3 that last for a few microseconds (see the subsequent signals at $20\,\mu\mathrm{s}$ - $50\,\mu\mathrm{s}$ of Figure 2(b) in Rison et al. (2016)). The results in Figure 3(d) show that by considering the extra long decay current I_{extra} and the simulation-estimated angle $\theta = 15°$ with respect to the z-axis, the tail parts of the electrostatic and induction components for NBE3 have been reduced, resulting in a better agreement with the observation (see Figure 3(b) and (d)). In this case, the estimated charge moment change Q_{mom} of the NBE3 is $-219\,\mathrm{C}\cdot\mathrm{m}$, which is similar to that of vertical NBE1.

Figure S4 in Supporting Information further shows the current distribution along the channel based on the rebounding MTLE model for the vertical NBE1, the vertical NBE3, and the slanted NBE3 without and with the extra current I_{extra}. We see that, among all cases, considering the inclination of the channel and the extra long decay current I_{extra} results in the best agreement with the INTF traces. This is consistent with the observations showing substantial azimuthal spread indicating a tilted channel.

4.3 Comparison with the observations reported by Karunarathne et al. (2016)

In this section, we compare the simulated results obtained by the slanted rebounding wave model with the electric fields measured by a FA array for the vertical and slanted cases reported by Karunarathne et al. (2016). In their study, Karunarathne et al. (2016) estimated three-dimensional charge moments of ten NBEs based on a dipole model and found that seven NBEs were essentially vertically oriented, while three NBEs were tilted at angles ranging from 10 to 20 degrees from the vertical. To further investigate the effect of the inclination in the NBE channel, we have chosen two cases: (i) NBE#174 corresponding to a vertical channel, and (ii) NBE#92 corresponding to a tilted channel.

Similar to the previous simulations, we consider the fast breakdown of NBEs as a system of positive streamers that propagate downwards along a distance L, then upwards back along the previous path, following the rebounding MTLE model (Li, Luque, Gordillo-Vázquez, et al., 2022). Since the fast breakdowns for both NBE#174 and NBE#92 are followed by slow electrostatic changes, in the simulation, we add the extra long decay current I_{extra} to address the effect of these slow electrostatic changes according to Equation (6).

As shown in Figure 4, for the vertical case NBE#174, with a polar angle $\theta = 0°$, the simulated results considering the extra long decay current I_{extra} agree well with the electric fields measured by different fast antennas located at distances from 9 km to 70 km. To compare our modeling results with those of Karunarathne et al. (2016), we assumed a channel length of 1000 m and a propagation velocity of $v = 2.6 \times 10^7$ m/s, both taken form the literature (Rison et al., 2016; Karunarathne et al., 2016). The best-fit parameters listed in Table S1 in Supporting Information are consistent with those reported by Karunarathne et al. (2016). It is worth noting that although Karunarathne et al. (2016) modeled NBE#174 in their study, they were unable to accurately reproduce the slow electrostatic changes at close stations since they assumed a current for the slow electrostatic change that linearly decreases with time. However, in our case, the observed electrostatic change can be explained by introducing an extra current I_{extra} that follows a double-exponential expression, which suggests that the current of the electrostatic change may actually decrease exponentially, rather than linearly.

The results illustrated in Figure 5(a,c,e,g) indicate that by assuming a vertical channel for the slanted case of NBE#92, the simulation does not agree well with the tail part of the observations at close distances, but shows a reasonable agreement beyond a distance of about 10 km. As previously mentioned, this is likely due to the inclination of the NBE sources, as supported by the results shown in Figure 5(b,d,f,h). From Figure 5, we see that when the simulation-estimated angle $\theta = 13°$ with respect to the Z axis is taken into account, the modeling of the tail part corresponding to the electrostatic component improves, resulting in a better agreement with both close and far observations.

The current distribution based on the rebounding MTLE model for the vertical NBE#174, the vertical NBE#92 and the slanted NBE#92 are given in Figure S5 in Supporting Information with the detailed inferred parameters given in Table S1 in Supporting Information. The model-estimated charge moment Q_{mom} for NBE#92 changed from $-4519\,\mathrm{C\cdot m}$ to $-6958\,\mathrm{C\cdot m}$ when considering the vertical channel instead of the slanted channel. Although our rebounding-wave model is capable of modeling the rebounding features inside the waveform, the rebounding wave feature for NBE#92 is not obvious due to the strong downward attenuation rate λ_d.

5 conclusions

In this study, we investigated the propagation effect of slanted NBE sources by using a new rebounding-wave model based on the slanted transmission line model. The modeling results were first validated against the full-wave FDTD method, and then compared with the observations for both vertical and slanted cases reported in the literature.

The inclination of the NBE channel significantly affects the electrostatic, induction, and radiation components of the electric fields at close distances ($d < 10\,\mathrm{km}$). However, the effect gets weaker at far distances ($d > 50\,\mathrm{km}$) where the fields are dominated by the radiation component. The effect of an inclination less than 30° becomes weak beyond a distance of about 10 km. However, the effect of slant angles bigger than 30° can not be ignored even at a distance of 50 km. For all the slanted cases, the proposed model considering the channel inclination improves the agreement with respect to a purely vertical channel.

Additionally, the effect of the slow electrostatic change following the NBEs was discussed. The results that consider the extra long decay current based on a double-exponential expression match well with the slow electrostatic change in both close and far observations. This suggests that the current of the slow electrostatic change may actually decrease exponentially, rather than linearly.

Apart from the NBE cases discussed in this study, the suggested equations can be applied to arbitrary observation distances, and, by approximating a curved channel geometry with piecewise linear segments, it can be further extended to any discharge shape.

Acknowledgments

The authors would like to thank Dr. Thomas C. Marshall, Dr. Sumedhe Karunarathne and Dr. Maribeth Stolzenburg at the University of Mississippi for providing data from Karunarathne et al. (2016). This work was supported by the European Research Council (ERC) under the European Union H2020 programme/ERC grant agreement 681257. Additionally, this work was supported by the Spanish Ministry of Science and Innovation, MINECO, under the project PID2019-109269RB-C43 and FEDER program. D.L. would like to acknowledge the Independent Research Fund Denmark (Danmarks Frie Forskningsfond) under grant agreement 1026-00420B. D.L., A.L. and F.J.G.V. acknowledge financial support from the State Agency for Research of the Spanish MCIU through the 'Center of Excellence Severo Ochoa' award for the Instituto de Astrofísica de Andalucía (SEV-2017-0709).

Open Research

The data that support the findings of this study are openly available in `https://doi.org/10.5281/zenodo.8069595`.

References

Abouzeid, G., Said I.and Shabib, & Zein El Dein, A. (2015). Analysis of Electromagnetic Fields Generated by Inclined Lightning Channel. *Arabian Journal for Science and Engineering*, *40*(9), 2585–2608. doi: 10.1007/s13369-015-1660-7

Attanasio, A., da Silva, C., & Krehbiel, P. (2021). Electrostatic Conditions That Produce Fast Breakdown in Thunderstorms. *Journal of Geophysical Research: Atmospheres*, *126*(19), e2021JD034829. doi: https://doi.org/10.1029/2021JD034829

Attanasio, A., Krehbiel, P. R., & da Silva, C. L. (2019). Griffiths and Phelps Lightning Initiation Model, Revisited. *Journal of Geophysical Research: Atmospheres*, *124*(14), 8076-8094. doi: 10.1029/2019JD030399

da Silva, C. L., Merrill, R. A., & Pasko, V. P. (2016a). Mathematical constraints on the use of transmission line models to investigate the preliminary breakdown stage of lightning flashes. *Radio Science*, *51*(5), 367-380. doi: https://doi.org/10.1002/2015RS005853

da Silva, C. L., Merrill, R. A., & Pasko, V. P. (2016b, May). Mathematical constraints on the use of transmission line models to investigate the preliminary breakdown stage of lightning flashes. *Radio Science*, *51*(5), 367–380. doi: 10.1002/2015RS005853

Eack, K. B. (2004). Electrical characteristics of narrow bipolar events. *Geophysical Research Letters*, *31*(20). doi: 10.1029/2004GL021117

Karunarathne, S., Marshall, T. C., Stolzenburg, M., & Karunarathna, N. (2016). Electrostatic field changes and durations of narrow bipolar events. *Journal of Geophysical Research: Atmospheres*, *121*(17), 10,161-10,174. doi: https://doi.org/10.1002/2016JD024789

Kostinskiy, A. Y., Marshall, T. C., & Stolzenburg, M. (2020). The Mechanism of the Origin and Development of Lightning From Initiating Event to Initial Breakdown Pulses (v.2). *Journal of Geophysical Research: Atmospheres*, *125*(22), e2020JD033191. doi: https://doi.org/10.1029/2020JD033191

Le Vine, D. M., & Meneghini, R. (1978a, May). Electromagnetic fields radiated from a lightning return stroke: Application of an exact solution to Maxwell's equations. , *83*(C5), 2377-2384. doi: 10.1029/JC083iC05p02377

Le Vine, D. M., & Meneghini, R. (1978b, sep). Simulation of radiation from lightning return strokes: The effects of tortuosity. *Radio Science*, *13*(5), 801-809. doi: 10.1029/RS013i005p00801

Le Vine, D. M. (1980). Sources of the strongest RF radiation from lightning. *Journal of Geophysical Research: Oceans*, *85*(C7), 4091-4095. doi: https://doi.org/10.1029/JC085iC07p04091

Li, D., Azadifar, M., Rachidi, F., Rubinstein, M., Diendorfer, G., Sheshyekani, K., … Wang, Z. (2016). Analysis of lightning electromagnetic field propagation in mountainous terrain and its effects on ToA-based lightning location systems. *Journal of Geophysical Research: Atmospheres*, *121*(2), 895-911. doi: 10.1002/2015JD024234

Li, D., Luque, A., Gordillo-Vazquez, F. J., Pérez-Invernón, F. J., Husbjerg, L. S., Neubert, T., … Reglero, V. (2023). Different Types of Corona Discharges Associated With High-Altitude Positive Narrow Bipolar Events Nearby Cloud Top. *Journal of Geophysical Research: Atmospheres*, *128*(4), e2022JD037883. doi: https://doi.org/10.1029/2022JD037883

Li, D., Luque, A., Gordillo-Vázquez, F. J., Silva, C. d., Krehbiel, P. R., Rachidi, F., & Rubinstein, M. (2022). Secondary fast breakdown in narrow bipolar events. *Geophysical Research Letters*, *49*(7), e2021GL097452. doi: https://doi.org/10.1029/2021GL097452

Li, D., Luque, A., Lehtinen, N. G., Gordillo-Vázquez, F. J., Neubert, T., Lu, G., … Reglero, V. (2022). Multi-Pulse Corona Discharges in Thunderclouds Observed in Optical and Radio Bands. *Geophysical Research Letters*, *49*(13), e2022GL098938. doi: https://doi.org/10.1029/2022GL098938

Li, D., Rubinstein, M., Rachidi, F., Diendorfer, G., Schulz, W., & Lu, G. (2017). Location Accuracy Evaluation of ToA-Based Lightning Location Systems Over Mountainous Terrain. *Journal of Geophysical Research: Atmospheres*, *122*(21), 11,760-11,775. doi: 10.1002/2017JD027520

Lyu, F., Cummer, S. A., Qin, Z., & Chen, M. (2019). Lightning Initiation Processes Imaged With Very High Frequency Broadband Interferometry. *Journal of Geophysical Research: Atmospheres*, *124*(6), 2994-3004. doi: 10.1029/2018JD029817

Marshall, R. A., da Silva, C. L., & Pasko, V. P. (2015, July). Elve doublets and compact intracloud discharges. , *42*(14), 6112–6119. doi: 10.1002/2015GL064862

Marshall, T., Bandara, S., Karunarathne, N., Karunarathne, S., Kolmasova, I., Siedlecki, R., & Stolzenburg, M. (2019). A study of lightning flash initiation prior to the first initial breakdown pulse. *Atmospheric Research*, *217*, 10-23. doi: https://doi.org/10.1016/j.atmosres.2018.10.013

Marshall, T., Stolzenburg, M., Karunarathna, N., & Karunarathne, S. (2014). Electromagnetic activity before initial breakdown pulses of lightning. *Journal of Geophysical Research: Atmospheres*, *119*(22), 12,558-12,574. doi: https://doi.org/10.1002/2014JD022155

Nag, A., & Rakov, V. A. (2010). Compact intracloud lightning discharges: 1. Mechanism of electromagnetic radiation and modeling. *Journal of Geophysical Research: Atmospheres*, *115*(D20). doi: 10.1029/2010JD014235

Nucci, C. A., & Rachidi, F. (1989). Experimental validation of a modification to the Transmission Line model for LEMP calculation. In *8th symposium and technical exhibition on electromagnetic compatibility, zurich, switzerland.*

Phelps, C. (1974). Positive streamer system intensification and its possible role in lightning initiation. *Journal of Atmospheric and Terrestrial Physics*, *36*(1), 103 - 111. doi: https://doi.org/10.1016/0021-9169(74)90070-1

Phelps, C., & Griffiths, R. F. (1976). Dependence of positive corona streamer propagation on air pressure and water vapor content. *Journal of Applied Physics*, *47*(7), 2929-2934. doi: 10.1063/1.323084

Rachidi, F., & Nucci, C. (1990). On the Master, Uman, Lin, Standler and the modified transmission line lightning return stroke current models. *Journal of Geophysical Research: Atmospheres*, *95*(D12), 20389-20393. doi: 10.1029/JD095iD12p20389

Rison, W., Krehbiel, P. R., Stock, M. G., Edens, H. E., Shao, X.-M., Thomas, R. J., . . . Zhang, Y. (2016). Observations of narrow bipolar events reveal how lightning is initiated in thunderstorms. *Nature communications*, *7*, 10721. doi: 10.1038/ncomms10721(2016)

Rubinstein, M., & Uman, M. A. (1990). On the radiation field turn-on term associated with traveling current discontinuities in lightning. *Journal of Geophysical Research: Atmospheres*, *95*(D4), 3711-3713. doi: 10.1029/JD095iD04p03711

Shao, X.-M., Fitzgerald, T. J., & Jacobson, A. R. (2005). Reply to comment by Rajeev Thottappillil and Vladimir A. Rakov on "Radio frequency radiation beam pattern of return strokes: A revisit to theoretical analysis". *Journal of Geophysical Research: Atmospheres*, *110*(D24). doi: 10.1029/2005JD005889

Shao, X.-M., Jacobson, A. R., & Fitzgerald, T. J. (2004). Radio frequency radiation beam pattern of lightning return strokes: A revisit to theoretical analysis. *Journal of Geophysical Research: Atmospheres*, *109*(D19). doi: 10.1029/2004JD004612

Smith, D. A., Heavner, M. J., Jacobson, A. R., Shao, X. M., Massey, R. S., Sheldon, R. J., & Wiens, K. C. (2004). A method for determining intracloud lightning and ionospheric heights from VLF/LF electric field records. *Radio Science*, *39*(1), RS1010. doi: 10.1029/2002RS002790

Smith, D. A., Shao, X. M., Holden, D. N., Rhodes, C. T., Brook, M., Krehbiel, P. R., . . . Thomas, R. J. (1999). A distinct class of isolated intracloud lightning discharges and their associated radio emissions. *Journal of Geophysical Research: Atmospheres*, *104*(D4), 4189-4212. doi: 10.1029/1998JD200045

Thottappillil, R., & Rakov, V. (2001). On the computation of electric fields from a lightning discharge in time domain. In *2001 IEEE EMC international symposium on electromagnetic compatibility* (Vol. 2, pp. 1030–1035).

Thottappillil, R., & Rakov, V. A. (2005). Comment on "Radio frequency radiation beam pattern of lightning return strokes: A revisit to theoretical analysis" by Xuan-Min Shao, Abram R. Jacobson, and T. Joseph Fitzgerald, journal = Journal of Geophysical Research: Atmospheres. , *110*(D24). doi: 10.1029/2004JD005729

Thottappillil, R., Uman, M. A., & Rakov, V. A. (1998). Treatment of retardation effects in calculating the radiated electromagnetic fields from the lightning discharge. *Journal of Geophysical Research: Atmospheres*, *103*(D8), 9003-9013. doi: 10.1029/97JD02941

Tilles, J. N., Liu, N., Stanley, M. A., Krehbiel, P. R., Rison, W., Stock, M. G., . . . Wilson, J.

(2019). Fast negative breakdown in thunderstorms. *Nature communications*, *10*(1), 1648. doi: 10.1038/s41467-019-09621-z

Uman, M. A., & McLain, D. K. (1970). Radiation field and current of the lightning stepped leader. *Journal of Geophysical Research (1896-1977)*, *75*(6), 1058-1066. doi: 10.1029/JC075i006p01058

Uman, M. A., McLain, D. K., & Krider, E. P. (1975). The electromagnetic radiation from a finite antenna. *American Journal of Physics*, *43*(1), 33-38. doi: 10.1119/1.10027

Uman, M. A., Martin A., & McLain, D. K. (1970). Lightning return stroke current from magnetic and radiation field measurements. *Journal of Geophysical Research (1896-1977)*, *75*(27), 5143-5147. doi: 10.1029/JC075i027p05143

Watson, S. S., & Marshall, T. C. (2007). Current propagation model for a narrow bipolar pulse. *Geophysical Research Letters*, *34*(4). doi: 10.1029/2006GL027426

427 # Figure list

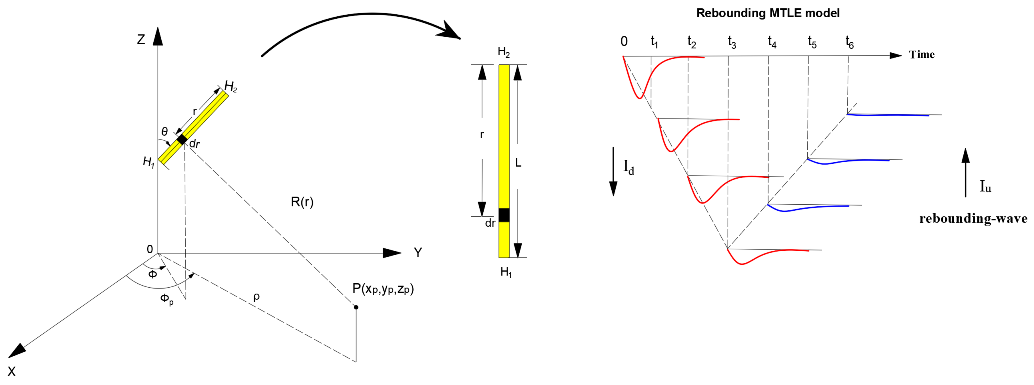

Figure 1. Geometry of the inclined NBE channel with a current that propagates following the rebounding MTLE model. (a) We model the NBE channel as a series of small straight segments at a radial distance of r and a polar angle θ with respect to the Z axis. The azimuth angle ϕ is defined by the angle between the X axis and the projection of the segment in the XY plane. The observation point $P(x_p, y_p, z_p)$ is at an altitude z_p above the ground surface and at a plane distance ρ from the source, thus $x_p = \rho\cos(\phi_p)$, $y_p = \rho\sin(\phi_p)$, where ϕ_p is the azimuth angle of the observation point P. (b) In the rebounding MTLE model, the NBE channel is considered as a system of positive streamer coronas that propagate downward from an altitude H_2 to H_1 with a channel length L, followed by upward negative streamer corona discharges that propagate back along the same path. Here, I_d is the downward current and I_u is the rebounding-wave current.

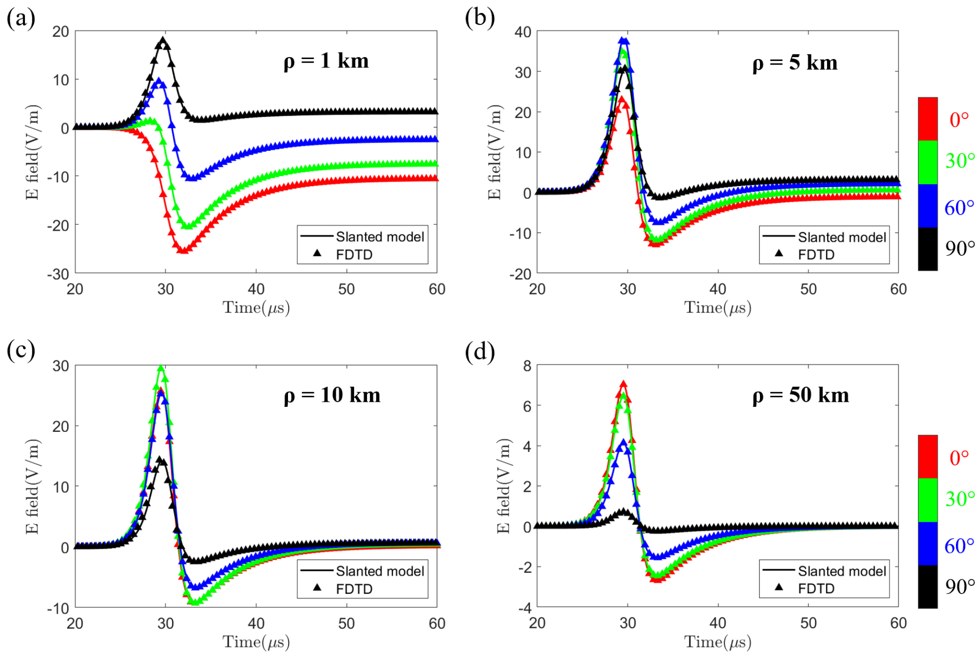

Figure 2. Comparison between the slanted rebounding wave model and FDTD method by considering the slanted dipole with different θ angles with respect to the z-axis and the azimuthal angle ϕ = 0° at a distance of 1 km, 5 km, 10 km and 50 km.

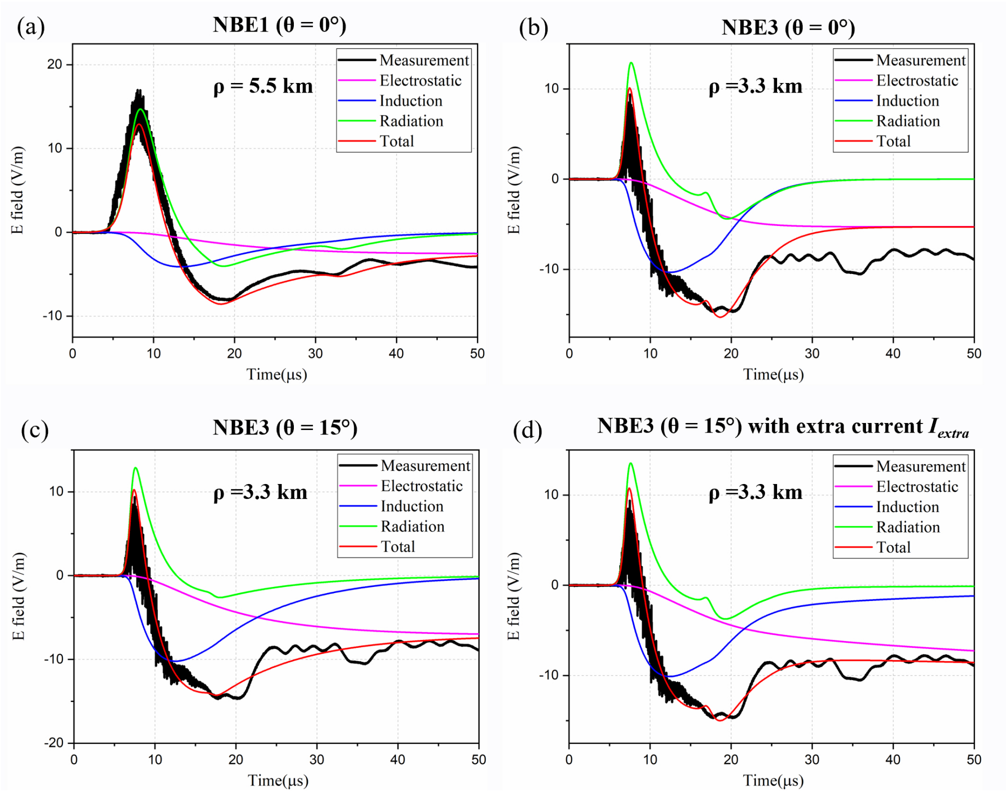

Figure 3. Comparison between the observations from Rison et al. (2016) and simulation results by assuming the vertical channel for NBE1(a) and NBE3(b) and the slanted channel for NBE3 without (c) and with (d) the extra current I_{extra}. The electrostatic, induction and radiation components of the total electric fields are also given in the figure.

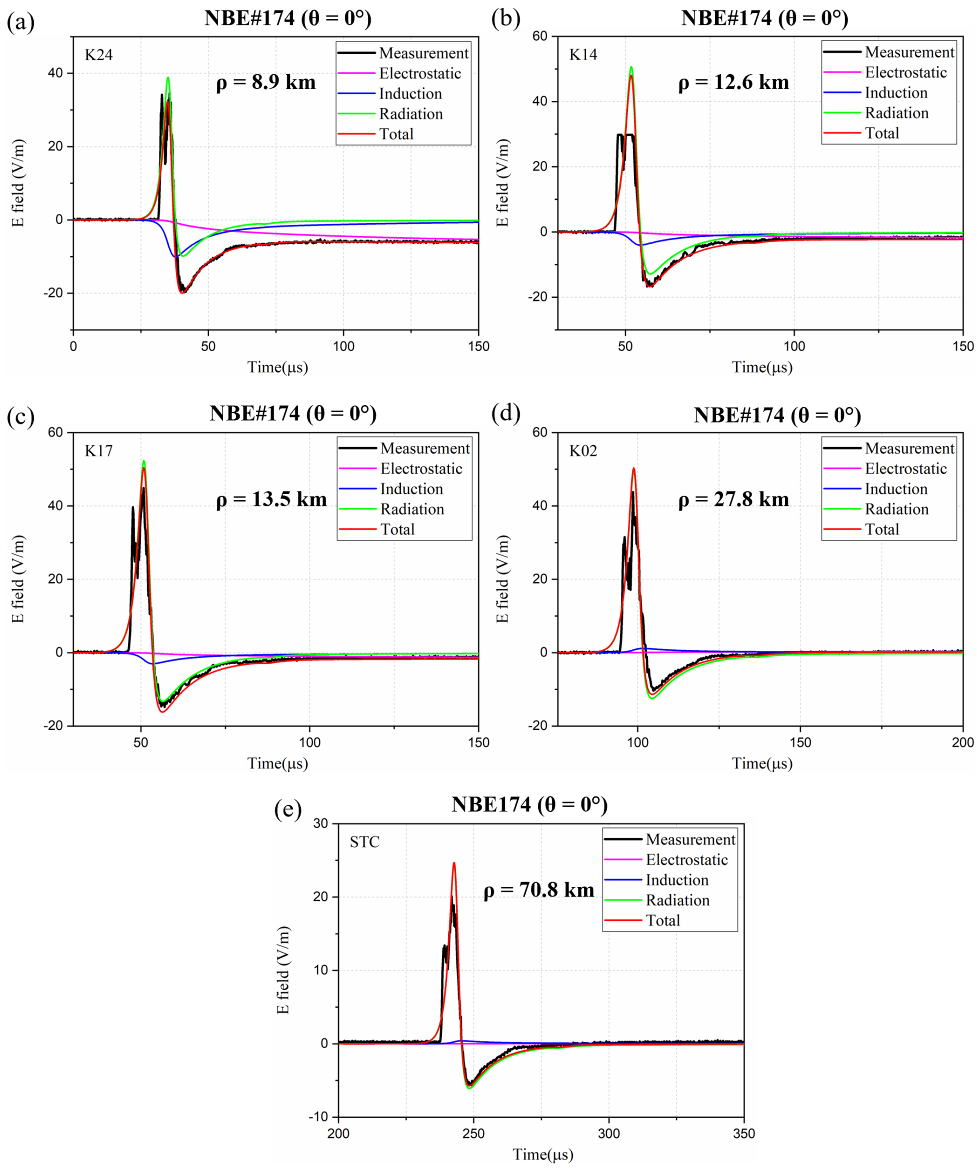

Figure 4. Comparison between the observations from Karunarathne et al. (2016) and simulation results by assuming a vertical channel for NBE#174 at different distances. The electrostatic, induction and radiation components of the total electric fields are also given in the figure.

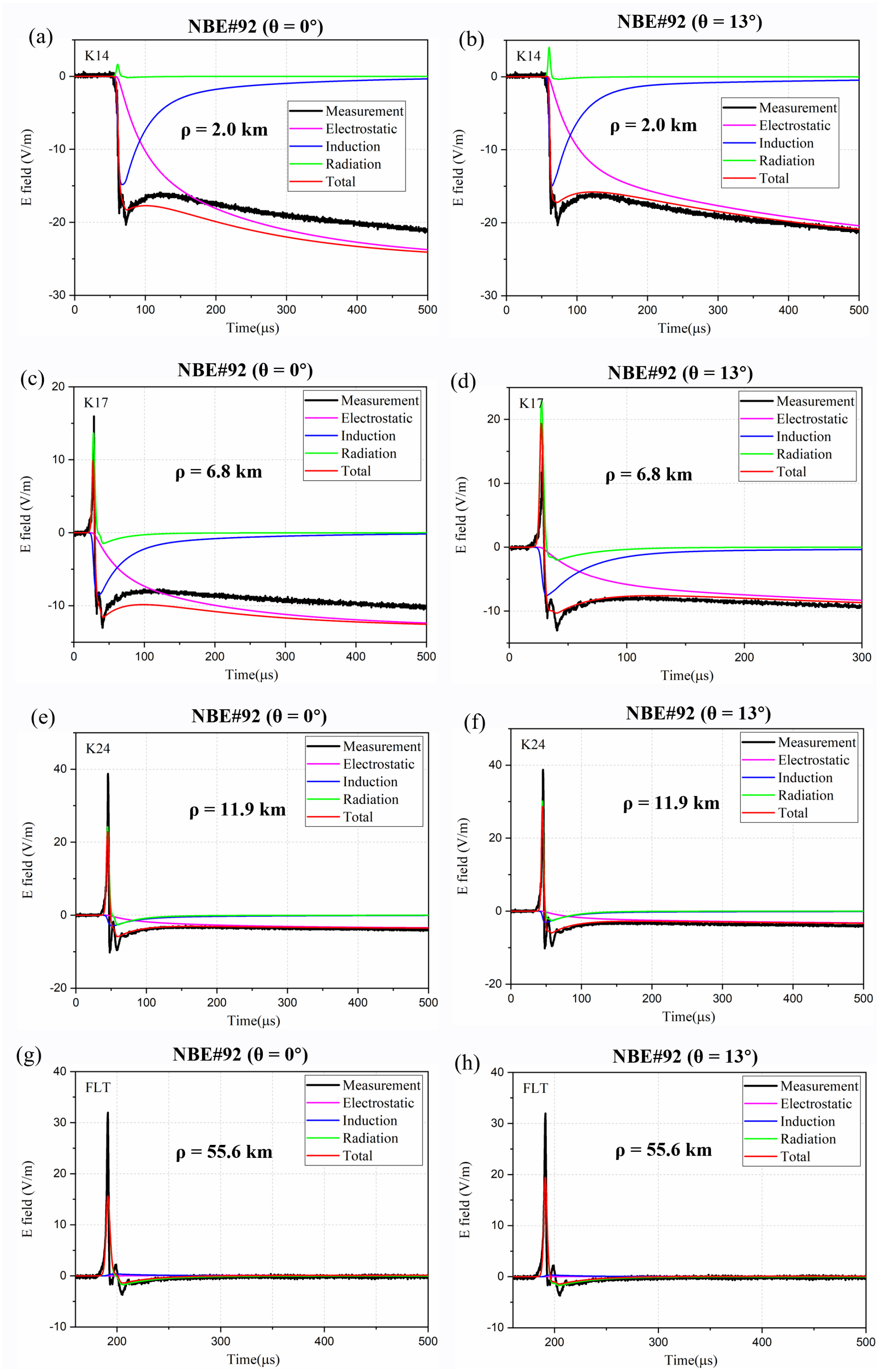

Figure 5. Comparison between the observations from Karunarathne et al. (2016) and simulation results by assuming a vertical channel (a,c,e,g) and a slanted channel (b,d,f,h) for NBE#92 at different distances. The electrostatic, induction and radiation components of the total electric fields are also given in the figure.

Propagation Effects of Slanted Narrow Bipolar Events: A Rebounding-Wave Model Study

Dongshuai Li[1,2], Alejandro Luque[2], Farhad Rachidi[3], Marcos Rubinstein[4], Torsten Neubert[1], Yanan Zhu[5], Olivier Chanrion[1], Caitano da Silva[6], Paul R. Krehbiel[6]

[1]National Space Institute, Technical University of Denmark (DTU Space), Kongens Lyngby, Denmark.
[2]Instituto de Astrofísica de Andalucía (IAA), CSIC, Granada, Spain.
[3]Electromagnetic Compatibility Laboratory, Swiss Federal Institute of Technology (EPFL), Lausanne, Switzerland.
[4]University of Applied Sciences and Arts Western Switzerland, Yverdon-les-Bains, Switzerland.
[5]Earth Networks, Germantown, Maryland, USA.
[6]Langmuir Laboratory for Atmospheric Research, New Mexico Institute of Mining and Technology, Socorro, USA.

Key Points:

- The propagation effect of slanted NBEs at different distance is investigated and compared with the observations.
- The inclination of the NBEs could significantly affect the electromagnetic fields in the close distance.
- The proposed equations will improve the quality of inferred features of slanted NBEs and can be extended to any discharge shape.

Corresponding author: Dongshuai Li[1,2] and Alejandro Luque[2],

[1] National Space Institute, Technical University of Denmark (DTU Space), Kongens Lyngby, Denmark.

[2] Instituto de Astrofísica de Andalucía (IAA), CSIC, Granada, Spain., (dongshuai@space.dtu.dk, aluque@iaa.es)

Abstract

Narrow bipolar events (NBEs) are impulsive and powerful intracloud discharges. Recent observations indicate that some NBEs exhibit a slanted orientation rather than strictly vertical. However, the inclination of NBEs has not been considered in previous transmission line models, leading to uncertainty when evaluating their characteristics based on electromagnetic fields. This paper investigates the propagation effects of slanted NBEs using a newly developed slanted rebounding-wave model. It is found that the calculated results using the proposed model match well with measurements for both vertical and slanted NBE cases. The inclination of the NBEs significantly affects the electromagnetic fields at close distances, while the effects weaken as the observation distance increases, where the fields are dominated by the radiation component. The slanted rebounding-wave model improves the agreement with respect to a purely vertical channel and can be extended to any discharge geometry at arbitrary observation distances.

Plain Language Summary

Narrow Bipolar Events (NBEs) are unique intracloud discharges that occur either individually or as the initiation event for lightning flashes inside thunderstorms. Knowing the physical mechanisms of NBEs will help us to better understand how lightning initiates inside thunderstorms. Recent studies indicated that NBEs could exhibit a slanted orientation rather than being strictly vertical. Here, in the light of these observations, we analyze the propagation effect of the slanted NBEs by using a newly developed slanted rebounding-wave model, and we compare the modeling results with observations. This study contributes to a better understanding of the physical mechanism of NBEs and provides a reference for accurately characterizing NBEs based on their electromagnetic fields.

1 introduction

In recent years, significant attention has been given to Narrow Bipolar Events (NBEs) due to their important role in lightning initiation (Rison et al., 2016; Tilles et al., 2019; Lyu et al., 2019). NBEs are generated by the intracloud discharges that emit strong radiation in the high and very high frequency (HF/VHF) range (Le Vine, 1980; Smith et al., 1999, 2004), and they are characterized by fast breakdowns (FBs) that appear to be a system of streamer coronas (Rison et al., 2016; Phelps, 1974; Phelps & Griffiths, 1976; Attanasio et al., 2021; Tilles et al., 2019; Lyu et al., 2019; Attanasio et al., 2019). However, the exact physical mechanism behind NBEs still remains unclear.

The transmission line model is widely recognized as the most commonly used approach for inferring the characteristics of NBEs based on their electromagnetic fields. NBEs typically have channel lengths ranging from hundreds of meters to a few kilometers (Smith et al., 1999, 2004). When observing NBEs at distances as large as hundreds of kilometers, only the radiation field component is observable. Therefore, many studies simplify the NBE channel by assuming it to be an infinitesimally short dipole (Smith et al., 1999, 2004; Eack, 2004). This has led to misinterpretation of electric current intensities in all types of pulses taking place during the initial breakdown stage of lightning, as discussed by da Silva et al. (2016b). However, for close-range observations within a few kilometers or less, where induction and electrostatic fields are also significant, more accurate transmission line-based models of NBEs are proposed in the literature. These models include the classic transmission line (TL) model (Watson & Marshall, 2007), the modified transmission line with exponential increase (MTLEI) model (Watson & Marshall, 2007), the bouncing-wave transmission line model (Nag & Rakov, 2010), the modified transmission line with exponential decay (MTLE) model (Rison et al., 2016; Karunarathne et al., 2016) and the modified transmission line-gaussian (MTLG) model (da Silva et al., 2016a; R. A. Marshall et al., 2015). Attanasio et al. (2021) argued that, from an electrostatic standpoint, the precursor streamer system can produce a strong electric field enhancement ahead of itself that may trigger a rebounding opposite-polarity event traveling back towards the origin. Recently, Li, Luque, Gordillo-Vázquez, et al. (2022) introduced a rebounding-wave model based on the Modified Transmission Line with Exponential decay (MTLE) model (Nucci & Rachidi, 1989; Rachidi & Nucci, 1990; Rison et al., 2016), termed "rebounding MTLE model", to represent the subsequent streamer features involved in NBEs (Rison et al., 2016;

Tilles et al., 2019; Attanasio et al., 2021). A common feature of all the transmission line-based models is the assumption that the NBE channel is vertically oriented.

Recent observations indicate that NBEs could be tilted from vertical and exhibit a noticeable spread in azimuthal values (Rison et al., 2016). Karunarathne et al. (2016) estimated the three-dimensional charge moments of ten NBEs and found that three of them were tilted at angles ranging from 10 to 20 degrees from the vertical. R. A. Marshall et al. (2015) suggested that slanted NBEs play a role in the illumination of the lower ionosphere known as "elve doublets". Particularly, these authors suggested that if the NBE source current is inclined towards the observer, the second elve in the doublet can be brighter than the first. However, the impact of channel inclination on the propagation effects of NBEs at different distances remains unknown. Here, following previous studies on the effect of the inclination and tortuosity of lightning return stroke channels (Le Vine & Meneghini, 1978b,a; Abouzeid & Zein El Dein, 2015), we propose an extension of the rebounding wave model of Li, Luque, Gordillo-Vázquez, et al. (2022) for NBEs. The so-called slanted rebounding wave model is firstly validated against a full-wave three-dimensional Finite-Difference Time-Domain (FDTD) method and then through comparisons with observations reported in the literature.

2 Slanted rebounding wave model

The slanted transmission line model was firstly proposed by Abouzeid & Zein El Dein (2015) to analyze the effect of lightning return stroke channel tortuosity and branching. In this study, we extend their equations to investigate the inclination of the NBE channel. NBE is considered as a system of streamer coronas represented by the a rebounding-wave model based on the Modified Transmission Line with Exponential decay (MTLE) (Nucci & Rachidi, 1989; Rachidi & Nucci, 1990; Rison et al., 2016), termed "rebounding MTLE model" (Li, Luque, Gordillo-Vázquez, et al., 2022).

As illustrated in Figure 1, the positive streamer coronas propagate downwards from an altitude H_2 to an altitude H_1 with a channel length L (for a slanted channel $H_1 = H_2 - r\cos\theta$), followed by upward negative streamer corona discharges that propagate back along the same path. I_d is the downward current (red color) and I_u is the rebounding-wave current (blue color). According to the rebounding MTLE model (Li, Luque, Gordillo-Vázquez, et al., 2022), the total current $I(r,t)$ is the sum of the downward current $I_d(r,t)$ and the upward rebounding current $I_u(r,t)$. Both currents are assumed to experience an exponential decay along the same propagation channel with attenuation rates of λ_d and λ_u, respectively. The total current and the downward and upward rebounding currents are given by

$$
\begin{aligned}
I(r,t) &= I_d(r,t) + I_u(r,t),\\
I_d(r,t) &= I(t-(L-r)/v_d)e^{-(L-r)/\lambda_d},\\
I_u(r,t) &= I(t-L/v_d-r/v_u)e^{-L/\lambda_d}e^{-r/\lambda_u},
\end{aligned}
\tag{1}
$$

where v_d and v_u are the downward and upward propagation velocities. The factor e^{-L/λ_d} ensures the continuity between the downward and the upward-propagating currents.

In free space, the vertical electric field E_z at the observation point $P(x_p, y_p, z_p)$, where $x_p = \rho\cos(\phi_p)$ and $y_p = \rho\sin(\phi_p)$, due to a short inclined dipole dr carrying the current $I(r,t)$ located at a height $(H_2 - r\cos\theta)$ is given as:.

$$
\begin{aligned}
dE_{zc} = & \frac{dr}{4\pi\epsilon_0} \\
& \begin{pmatrix}
\begin{pmatrix}
\frac{3(z_p-(H_2-r\cos\theta))(x_p-r\sin\theta\cos\phi)}{R^5(r)} \sin\theta\cos\phi \\
+\frac{3(z_p-(H_2-r\cos\theta))(y_p-r\sin\theta\sin\phi)}{R^5(r)} \sin\theta\sin\phi \\
+\frac{3(z_p-(H_2-r\cos\theta))^2-R^2(r)}{R^5(r)} \cos\theta
\end{pmatrix} \int_0^t I(r,t)d\tau \\
\begin{pmatrix}
\frac{3(z_p-(H_2-r\cos\theta))(x_p-r\sin\theta\cos\phi)}{cR^4(r)} \sin\theta\cos\phi \\
+\frac{3(z_p-(H_2-r\cos\theta))(y_p-r\sin\theta\sin\phi)}{cR^4(r)} \sin\theta\sin\phi \\
+\frac{3(z_p-(H_2-r\cos\theta))^2-R^2(r)}{cR^4(r)} \cos\theta
\end{pmatrix} I(r,t) \\
\begin{pmatrix}
\frac{(z_p-(H_2-r\cos\theta))(x_p-r\sin\theta\cos\phi)}{c^2R^3(r)} \sin\theta\cos\phi \\
+\frac{(z_p-(H_2-r\cos\theta))(y_p-r\sin\theta\sin\phi)}{c^2R^3(r)} \sin\theta\sin\phi \\
+\frac{(z_p-(H_2-r\cos\theta))^2-R^2(r)}{c^2R^3(r)} \cos\theta
\end{pmatrix} \frac{\partial I(r,t)}{\partial t}
\end{pmatrix},
\end{aligned}
\tag{2}
$$

where,

$$
R(r) = \sqrt{(x_p - r\sin\theta\cos\phi)^2 + (y_p - r\sin\theta\sin\phi)^2 + (z_p - (H_2 - r\cos\theta))^2}. \tag{3}
$$

Individual terms on the right hand side of Equation (2) containing the factors are the electrostatic, induction and radiation components. If we assume the ground as a perfectly conducting plane, its effect can be taken into account using image theory, yielding

$$
\begin{aligned}
dE_{zm} = & -\frac{dr}{4\pi\epsilon_0} \\
& \begin{pmatrix}
\begin{pmatrix}
\frac{3(z_p+(H_2-r\cos\theta))(x_p-r\sin\theta\cos\phi)}{R_0^5(r)} \sin\theta\cos\phi \\
+\frac{3(z_p+(H_2-r\cos\theta))(y_p-r\sin\theta\sin\phi)}{R_0^5(r)} \sin\theta\sin\phi \\
-\frac{3(z_p+(H_2-r\cos\theta))^2-R_0^2(r)}{R_0^5(r)} \cos\theta
\end{pmatrix} \int_0^t I(r,t)d\tau \\
\begin{pmatrix}
\frac{3(z_p+(H_2-r\cos\theta))(x_p-r\sin\theta\cos\phi)}{cR_0^4(r)} \sin\theta\cos\phi \\
+\frac{3(z_p+(H_2-r\cos\theta))(y_p-r\sin\theta\sin\phi)}{cR_0^4(r)} \sin\theta\sin\phi \\
-\frac{3(z_p+(H_2-r\cos\theta))^2-R_0^2(r)}{cR^4(r)} \cos\theta
\end{pmatrix} I(r,t) \\
\begin{pmatrix}
\frac{(z_p+(H_2-r\cos\theta))(x_p-r\sin\theta\cos\phi)}{c^2R_0^3(r)} \sin\theta\cos\phi \\
+\frac{(z_p+(H_2-r\cos\theta))(y_p-r\sin\theta\sin\phi)}{c^2R_0^3(r)} \sin\theta\sin\phi \\
-\frac{(z_p+(H_2-r\cos\theta))^2-R_0^2(r)}{c^2R^3(r)} \cos\theta
\end{pmatrix} \frac{\partial I(r,t)}{\partial t}
\end{pmatrix},
\end{aligned}
\tag{4}
$$

where,

$$
R_0(r) = \sqrt{(x_p - r\sin\theta\cos\phi)^2 + (y_p - r\sin\theta\sin\phi)^2 + (z_p + (H_2 - r\cos\theta))^2}. \tag{5}
$$

For an observer P located on the ground surface, the height of the observation point z_p is equal to zero in all the equations above, implying $R = R_0$. The total vertical electric field E_z for the whole inclined channel can be obtained by integrating the dipole field dE_{zc} and its image dE_{zm} over the entire channel. Note that both the dipole field dE_{zc} and its image dE_{zm} include the slanted feature of the sources, and they reduce to the case of a vertical channel when the polar angle $\theta = 0$ (Thottappillil & Rakov, 2001; M. A. Uman et al., 1975). Moreover, the equations are not limited to straight channel but also can be applied to any arbitrarily tortuous discharge channel by approximating it as a series of small straight segments.

Although not mentioned in the study of Abouzeid & Zein El Dein (2015), the so-called discontinuity term (Thottappillil et al., 1998; Thottappillil & Rakov, 2001),“turn-on” term (M. A. Uman & McLain, 1970; M. A. Uman Martin A. & McLain, 1970) or F factor (Rubinstein & Uman, 1990; Thottappillil & Rakov, 2001, 2005; Shao et al., 2004, 2005) should be considered if there is a current discontinuity at the propagation wave front. The equations for the discontinuity term are given in Text S1 in Supporting Information.

3 Validation of the slanted rebounding wave model

To validate the proposed slanted transmission line equations for NBEs, we compare its prediction against a full-wave three-dimensional FDTD model (Li et al., 2016, 2017). In the simulation, the NBE source is assumed to be a dipole at an altitude $H = 5\,\text{km}$ above a perfectly conducting ground with different polar angle θ of 0°, 30°, 60° and 90°. The current waveform is given by double-exponential expression with $I(t) = I_0(e^{\alpha t}/(1 + e^{(\alpha+\beta)t})$, where the rise time constant is $\alpha = 1/\tau_1$ and the fall time constant is $\beta = 1/\tau_2$ (Rison et al., 2016). The values of τ_1 and τ_2 are 1 µs and 5 µs, respectively. The peak current is normalized to $I_{peak} = -100\,\text{kA}$ by setting $I_0 = I_{peak}(1 + \frac{\alpha}{\beta})(\frac{\alpha}{\beta})^{(\frac{-\alpha}{\alpha+\beta})}$.

For a vertical dipole with $\theta = 0°$, the electric field varies with azimuthal symmetry, but it is more complicated for the slanted cases showing different features depending on the different azimuthal angles. The comparison between the slanted rebounding wave model and the FDTD method for both vertical and slanted dipoles is given in Figure 2. The results calculated by the presented equations match perfectly with the FDTD results for both vertical and slanted sources. For horizontal dipole with $\theta = 90°$, the electric field first increases within a distance of 5 km and then decreases as the observer moves away from the source and becomes negligible beyond a distance of about 50 km.

The results from the FDTD simulation are further shown in Figure S1 and S2 in Supporting Information. Figure S1 shows the side view (a, c, e, g) and top view (b, d, f, h) of a snapshot of the FDTD simulation for the vertical electric fields of the slanted dipole with $\theta = 0°$, 30°, 60° and 90°. Figure S2 illustrates the electrostatic, induction and radiation components for both vertical and slanted dipoles at different distances. The inclination of the source at closer distances ($\leq$ 10 km) causes a significant effect on the electrostatic and induction components of the electric fields. Both the waveshape and the amplitude of the electric field are influenced by the inclination of the source (see Figure S2(d1, d2, d3)). In our case, the reversal distance (Nag & Rakov, 2010), where the electrostatic and induction components of the field reverse their polarity, varies as a function of the slanted dipole angle. As shown in Figure S2(d2, e2, d3 and e3), the tail part of the waveform becomes higher due to the increase of the electrostatic fields caused by the slant angle. For distances beyond 50 km, the electric field is dominated by the radiation component, and the inclination only affects the amplitudes (see Figure S2(d4 and e4)). It is interesting to note that the effect of the slant angle lower than 30° becomes weak beyond a distance of about 10 km. However, the effect of slant angles bigger than 30° could not be ignored even at distances as large as 50 km.

4 Comparison with the observations in the literature

4.1 The electrical discharges following NBEs

Recent studies reported that the electric fields of NBEs at distances below 10 km include two parts: a main bipolar pulse characteristic of NBE and a slow electrostatic change lasting from tens of microseconds to a few milliseconds (Karunarathne et al., 2016; T. Marshall et al., 2014). The slow electrostatic change following NBEs seems to be related to the attempted electrical activities that never developed into a full lightning flash (Karunarathne et al., 2016). This fact is also supported by the multi-pulse corona discharges observed by the Atmosphere-Space Interactions Monitor (ASIM) onboard International Space Station (ISS) (Li, Luque, Lehtinen, et al., 2022; Li et al., 2023). In their study, Li, Luque, Lehtinen, et al. (2022) found that, for the multi-pulse corona discharges, the first optical pulse coincides with a strong radio signal in the form of a NBE but subsequent optical pulses, delayed by some milliseconds, are related to horizontally oriented streamer-like electrical discharges which do not trigger full-fledged lightning. However, it remains unclear whether these electrical discharges following NBEs are part of the NBEs produced by the remaining streamer corona activities (Rison et al., 2016; Li, Luque, Gordillo-Vázquez, et al., 2022) or if they are independent electrical discharges, similar to the Initial E-Change (IEC) that occurs before the first initial breakdown pulses of a lightning flash (T. Marshall et al., 2014, 2019; Kostinskiy et al., 2020).

In our study, we consider these electrical discharges as an extra long decay current I_{extra} along with the main NBE current, despite lacking knowledge about their physical mechanism. The current is represented using the double-exponential expressions (Rison et al., 2016),

$$I(t) = I_{NBE}(t) + I_{extra}(t) = I_0 \frac{e^{\alpha t}}{1 + e^{(\alpha+\beta)t}} + \eta I_0 \frac{e^{\alpha t}}{1 + e^{(\alpha+\gamma)t}}, \tag{6}$$

where the rise time constant for the original streamer current $\alpha = 1/\tau_1$ and the fall time constant for the original streamer current $\beta = 1/\tau_2$. For the extra current $\gamma = 1/\tau_3$. $0 \le \eta \le 1$ is the fraction of the extra current $I_{extra}(t)$ compared to the primary NBE current $I_{NBE}(t)$. The peak value of I_{NBE} is normalized to I_{peak} by setting $I_0 = I_{peak}(1 + \frac{\alpha}{\beta})(\frac{\alpha}{\beta})^{(\frac{-\alpha}{\alpha+\beta})}$.

4.2 Comparison with the observations reported by Rison et al. (2016)

In this section, we compare the simulated results obtained by the slanted rebounding wave model with the electric fields measured by a fast antenna (FA) for the vertical and slanted cases reported by Rison et al. (2016). According to interferometer (INTF) observations, the NBEs consisted of a downward Fast Positive Breakdown (FPB) followed immediately by an upward Fast Negative Breakdown (FNB) that propagated back in the opposite direction along the previous path. In the simulation, we model the fast breakdown of the NBE as a system of positive streamers that propagate downwards over a distance L, then upwards back along the previous path as predicted by the rebounding MTLE model (Li, Luque, Gordillo-Vázquez, et al., 2022). The same double-exponential current is adopted for the comparison with the results of Rison et al. (2016).

According to Equation (1), the total current $I(r,t)$ is the sum of the downward current $I_d(r,t)$ and the upward rebounding current $I_u(r,t)$, where $v_d = L/t_d$ and $v_u = L/t_u$ are the downward and upward velocities related to the inferred downward and upward propagation times t_d and t_u obtained by fitting the INTF traces for both NBE1 and NBE3 with the best fit lines shown in Li, Luque, Gordillo-Vázquez, et al. (2022) (see Figure 2 there).

As mentioned by Rison et al. (2016), the NBE1 discharge occurred at constant azimuth consistent with the positive breakdown being vertically downward (see Figure 7 in the Supplementary Material of Rison et al. (2016)). On the other hand, NBE3 showed substantial azimuthal spread with nonnegligible tilt from vertical (see Figure 9 in the Supplementary Material of Rison et al. (2016)). Firstly, we assume the channel to be vertical ($\theta = 0$) for both NBE1 and NBE3. Note that the results by assuming both NBE1 and NBE3 to be vertical are discussed in Li, Luque, Gordillo-Vázquez, et al. (2022). Here we also present the results in Figure 3 with the best-fit parameters listed in Table S1 in Supporting Information. The estimated charge moment change Q_{mom} for the vertical NBE1 and vertical NBE3 are $-215\,\mathrm{C \cdot m}$ and $-116\,\mathrm{C \cdot m}$, respectively. It is found that the simulated results for NBE1 agree well with the observations. However, this is not the case for the slanted case of NBE3, for which significant deviations can be observed, especially in the tail part of the waveform.

In order to investigate the effect of the inclination of NBE sources on the fields, we introduce an additional free parameter, the polar angle θ, to represent the effect of inclination. To simplify the geometry, we assume that the plane containing the NBE channel is perpendicular to the transfer vector from the INTF observations' geometry to the geometry used in Figure 1 (see Text S2 and Figure S3 in Supporting Information). The azimuth angle for the source $\phi = 249°$ and for the observation point P, $\phi_p = 160°$, are estimated based on the transformation. The simulated result for the slanted NBE3 is presented in Figure 3(c) with the inferred features shown in Table S1 in Supporting Information. By considering the simulation-estimated polar angle of $\theta = 15°$, the simulated waveform for NBE3 reasonably agrees with the measurement, corresponding to a charge moment change of $-357\,\mathrm{C \cdot m}$, which is three times larger than the vertical case. However, the observed flattening tail part of NBE3 still could not be matched well. This suggests that NBE3 might involve more complicated processes than just being slanted.

As mentioned earlier, the electrostatic offset of NBE3 could be produced by the remaining streamer activities following NBEs (Rison et al., 2016). To address this, we introduce an additional long decay current, I_{extra}, derived from the presence of the remaining streamer corona activities of NBE3 that last for a few microseconds (see the subsequent signals at $20\,\mu\mathrm{s}$ - $50\,\mu\mathrm{s}$ of Figure 2(b) in Rison et al. (2016)). The results in Figure 3(d) show that by considering the extra long decay current I_{extra} and the simulation-estimated angle $\theta = 15°$ with respect to the z-axis, the tail parts of the electrostatic and induction components for NBE3 have been reduced, resulting in a better agreement with the observation (see Figure 3(b) and (d)). In this case, the estimated charge moment change Q_{mom} of the NBE3 is $-219\,\mathrm{C \cdot m}$, which is similar to that of vertical NBE1.

Figure S4 in Supporting Information further shows the current distribution along the channel based on the rebounding MTLE model for the vertical NBE1, the vertical NBE3, and the slanted NBE3 without and with the extra current I_{extra}. We see that, among all cases, considering the inclination of the channel and the extra long decay current I_{extra} results in the best agreement with the INTF traces. This is consistent with the observations showing substantial azimuthal spread indicating a tilted channel.

4.3 Comparison with the observations reported by Karunarathne et al. (2016)

In this section, we compare the simulated results obtained by the slanted rebounding wave model with the electric fields measured by a FA array for the vertical and slanted cases reported by Karunarathne et al. (2016). In their study, Karunarathne et al. (2016) estimated three-dimensional charge moments of ten NBEs based on a dipole model and found that seven NBEs were essentially vertically oriented, while three NBEs were tilted at angles ranging from 10 to 20 degrees from the vertical. To further investigate the effect of the inclination in the NBE channel, we have chosen two cases: (i) NBE#174 corresponding to a vertical channel, and (ii) NBE#92 corresponding to a tilted channel.

Similar to the previous simulations, we consider the fast breakdown of NBEs as a system of positive streamers that propagate downwards along a distance L, then upwards back along the previous path, following the rebounding MTLE model (Li, Luque, Gordillo-Vázquez, et al., 2022). Since the fast breakdowns for both NBE#174 and NBE#92 are followed by slow electrostatic changes, in the simulation, we add the extra long decay current I_{extra} to address the effect of these slow electrostatic changes according to Equation (6).

As shown in Figure 4, for the vertical case NBE#174, with a polar angle $\theta = 0°$, the simulated results considering the extra long decay current I_{extra} agree well with the electric fields measured by different fast antennas located at distances from 9 km to 70 km. To compare our modeling results with those of Karunarathne et al. (2016), we assumed a channel length of 1000 m and a propagation velocity of $v = 2.6 \times 10^7$ m/s, both taken form the literature (Rison et al., 2016; Karunarathne et al., 2016). The best-fit parameters listed in Table S1 in Supporting Information are consistent with those reported by Karunarathne et al. (2016). It is worth noting that although Karunarathne et al. (2016) modeled NBE#174 in their study, they were unable to accurately reproduce the slow electrostatic changes at close stations since they assumed a current for the slow electrostatic change that linearly decreases with time. However, in our case, the observed electrostatic change can be explained by introducing an extra current I_{extra} that follows a double-exponential expression, which suggests that the current of the electrostatic change may actually decrease exponentially, rather than linearly.

The results illustrated in Figure 5(a,c,e,g) indicate that by assuming a vertical channel for the slanted case of NBE#92, the simulation does not agree well with the tail part of the observations at close distances, but shows a reasonable agreement beyond a distance of about 10 km. As previously mentioned, this is likely due to the inclination of the NBE sources, as supported by the results shown in Figure 5(b,d,f,h). From Figure 5, we see that when the simulation-estimated angle $\theta = 13°$ with respect to the Z axis is taken into account, the modeling of the tail part corresponding to the electrostatic component improves, resulting in a better agreement with both close and far observations.

The current distribution based on the rebounding MTLE model for the vertical NBE#174, the vertical NBE#92 and the slanted NBE#92 are given in Figure S5 in Supporting Information with the detailed inferred parameters given in Table S1 in Supporting Information. The model-estimated charge moment Q_{mom} for NBE#92 changed from $-4519\,\mathrm{C}\cdot\mathrm{m}$ to $-6958\,\mathrm{C}\cdot\mathrm{m}$ when considering the vertical channel instead of the slanted channel. Although our rebounding-wave model is capable of modeling the rebounding features inside the waveform, the rebounding wave feature for NBE#92 is not obvious due to the strong downward attenuation rate λ_d.

5 conclusions

In this study, we investigated the propagation effect of slanted NBE sources by using a new rebounding-wave model based on the slanted transmission line model. The modeling results were first validated against the full-wave FDTD method, and then compared with the observations for both vertical and slanted cases reported in the literature.

The inclination of the NBE channel significantly affects the electrostatic, induction, and radiation components of the electric fields at close distances ($d < 10\,\mathrm{km}$). However, the effect gets weaker at far distances ($d > 50\,\mathrm{km}$) where the fields are dominated by the radiation component. The effect of an inclination less than 30° becomes weak beyond a distance of about 10 km. However, the effect of slant angles bigger than 30° can not be ignored even at a distance of 50 km. For all the slanted cases, the proposed model considering the channel inclination improves the agreement with respect to a purely vertical channel.

Additionally, the effect of the slow electrostatic change following the NBEs was discussed. The results that consider the extra long decay current based on a double-exponential expression match well with the slow electrostatic change in both close and far observations. This suggests that the current of the slow electrostatic change may actually decrease exponentially, rather than linearly.

Apart from the NBE cases discussed in this study, the suggested equations can be applied to arbitrary observation distances, and, by approximating a curved channel geometry with piecewise linear segments, it can be further extended to any discharge shape.

Acknowledgments

The authors would like to thank Dr. Thomas C. Marshall, Dr. Sumedhe Karunarathne and Dr. Maribeth Stolzenburg at the University of Mississippi for providing data from Karunarathne et al. (2016). This work was supported by the European Research Council (ERC) under the European Union H2020 programme/ERC grant agreement 681257. Additionally, this work was supported by the Spanish Ministry of Science and Innovation, MINECO, under the project PID2019-109269RB-C43 and FEDER program. D.L. would like to acknowledge the Independent Research Fund Denmark (Danmarks Frie Forskningsfond) under grant agreement 1026-00420B. D.L., A.L. and F.J.G.V. acknowledge financial support from the State Agency for Research of the Spanish MCIU through the 'Center of Excellence Severo Ochoa' award for the Instituto de Astrofísica de Andalucía (SEV-2017-0709).

Open Research

The data that support the findings of this study are openly available in `https://doi.org/10.5281/zenodo.8069595`.

References

Abouzeid, G., Said I.and Shabib, & Zein El Dein, A. (2015). Analysis of Electromagnetic Fields Generated by Inclined Lightning Channel. *Arabian Journal for Science and Engineering*, *40*(9), 2585–2608. doi: 10.1007/s13369-015-1660-7

Attanasio, A., da Silva, C., & Krehbiel, P. (2021). Electrostatic Conditions That Produce Fast Breakdown in Thunderstorms. *Journal of Geophysical Research: Atmospheres*, *126*(19), e2021JD034829. doi: https://doi.org/10.1029/2021JD034829

Attanasio, A., Krehbiel, P. R., & da Silva, C. L. (2019). Griffiths and Phelps Lightning Initiation Model, Revisited. *Journal of Geophysical Research: Atmospheres*, *124*(14), 8076-8094. doi: 10.1029/2019JD030399

da Silva, C. L., Merrill, R. A., & Pasko, V. P. (2016a). Mathematical constraints on the use of transmission line models to investigate the preliminary breakdown stage of lightning flashes. *Radio Science*, *51*(5), 367-380. doi: https://doi.org/10.1002/2015RS005853

da Silva, C. L., Merrill, R. A., & Pasko, V. P. (2016b, May). Mathematical constraints on the use of transmission line models to investigate the preliminary breakdown stage of lightning flashes. *Radio Science*, *51*(5), 367–380. doi: 10.1002/2015RS005853

Eack, K. B. (2004). Electrical characteristics of narrow bipolar events. *Geophysical Research Letters*, *31*(20). doi: 10.1029/2004GL021117

Karunarathne, S., Marshall, T. C., Stolzenburg, M., & Karunarathna, N. (2016). Electrostatic field changes and durations of narrow bipolar events. *Journal of Geophysical Research: Atmospheres*, *121*(17), 10,161-10,174. doi: https://doi.org/10.1002/2016JD024789

Kostinskiy, A. Y., Marshall, T. C., & Stolzenburg, M. (2020). The Mechanism of the Origin and Development of Lightning From Initiating Event to Initial Breakdown Pulses (v.2). *Journal of Geophysical Research: Atmospheres*, *125*(22), e2020JD033191. doi: https://doi.org/10.1029/2020JD033191

Le Vine, D. M., & Meneghini, R. (1978a, May). Electromagnetic fields radiated from a lightning return stroke: Application of an exact solution to Maxwell's equations. , *83*(C5), 2377-2384. doi: 10.1029/JC083iC05p02377

Le Vine, D. M., & Meneghini, R. (1978b, sep). Simulation of radiation from lightning return strokes: The effects of tortuosity. *Radio Science*, *13*(5), 801-809. doi: 10.1029/RS013i005p00801

Le Vine, D. M. (1980). Sources of the strongest RF radiation from lightning. *Journal of Geophysical Research: Oceans*, *85*(C7), 4091-4095. doi: https://doi.org/10.1029/JC085iC07p04091

Li, D., Azadifar, M., Rachidi, F., Rubinstein, M., Diendorfer, G., Sheshyekani, K., ... Wang, Z. (2016). Analysis of lightning electromagnetic field propagation in mountainous terrain and its effects on ToA-based lightning location systems. *Journal of Geophysical Research: Atmospheres*, *121*(2), 895-911. doi: 10.1002/2015JD024234

Li, D., Luque, A., Gordillo-Vazquez, F. J., Pérez-Invernón, F. J., Husbjerg, L. S., Neubert, T., ... Reglero, V. (2023). Different Types of Corona Discharges Associated With High-Altitude Positive Narrow Bipolar Events Nearby Cloud Top. *Journal of Geophysical Research: Atmospheres*, *128*(4), e2022JD037883. doi: https://doi.org/10.1029/2022JD037883

Li, D., Luque, A., Gordillo-Vázquez, F. J., Silva, C. d., Krehbiel, P. R., Rachidi, F., & Rubinstein, M. (2022). Secondary fast breakdown in narrow bipolar events. *Geophysical Research Letters*, *49*(7), e2021GL097452. doi: https://doi.org/10.1029/2021GL097452

Li, D., Luque, A., Lehtinen, N. G., Gordillo-Vázquez, F. J., Neubert, T., Lu, G., ... Reglero, V. (2022). Multi-Pulse Corona Discharges in Thunderclouds Observed in Optical and Radio Bands. *Geophysical Research Letters*, *49*(13), e2022GL098938. doi: https://doi.org/10.1029/2022GL098938

Li, D., Rubinstein, M., Rachidi, F., Diendorfer, G., Schulz, W., & Lu, G. (2017). Location Accuracy Evaluation of ToA-Based Lightning Location Systems Over Mountainous Terrain. *Journal of Geophysical Research: Atmospheres*, *122*(21), 11,760-11,775. doi: 10.1002/2017JD027520

Lyu, F., Cummer, S. A., Qin, Z., & Chen, M. (2019). Lightning Initiation Processes Imaged With Very High Frequency Broadband Interferometry. *Journal of Geophysical Research: Atmospheres*, *124*(6), 2994-3004. doi: 10.1029/2018JD029817

Marshall, R. A., da Silva, C. L., & Pasko, V. P. (2015, July). Elve doublets and compact intracloud discharges. , *42*(14), 6112–6119. doi: 10.1002/2015GL064862

Marshall, T., Bandara, S., Karunarathne, N., Karunarathne, S., Kolmasova, I., Siedlecki, R., & Stolzenburg, M. (2019). A study of lightning flash initiation prior to the first initial breakdown pulse. *Atmospheric Research*, *217*, 10-23. doi: https://doi.org/10.1016/j.atmosres.2018.10.013

Marshall, T., Stolzenburg, M., Karunarathna, N., & Karunarathne, S. (2014). Electromagnetic activity before initial breakdown pulses of lightning. *Journal of Geophysical Research: Atmospheres*, *119*(22), 12,558-12,574. doi: https://doi.org/10.1002/2014JD022155

Nag, A., & Rakov, V. A. (2010). Compact intracloud lightning discharges: 1. Mechanism of electromagnetic radiation and modeling. *Journal of Geophysical Research: Atmospheres*, *115*(D20). doi: 10.1029/2010JD014235

Nucci, C. A., & Rachidi, F. (1989). Experimental validation of a modification to the Transmission Line model for LEMP calculation. In *8th symposium and technical exhibition on electromagnetic compatibility, zurich, switzerland.*

Phelps, C. (1974). Positive streamer system intensification and its possible role in lightning initiation. *Journal of Atmospheric and Terrestrial Physics*, *36*(1), 103 - 111. doi: https://doi.org/10.1016/0021-9169(74)90070-1

Phelps, C., & Griffiths, R. F. (1976). Dependence of positive corona streamer propagation on air pressure and water vapor content. *Journal of Applied Physics*, *47*(7), 2929-2934. doi: 10.1063/1.323084

Rachidi, F., & Nucci, C. (1990). On the Master, Uman, Lin, Standler and the modified transmission line lightning return stroke current models. *Journal of Geophysical Research: Atmospheres*, *95*(D12), 20389-20393. doi: 10.1029/JD095iD12p20389

Rison, W., Krehbiel, P. R., Stock, M. G., Edens, H. E., Shao, X.-M., Thomas, R. J., … Zhang, Y. (2016). Observations of narrow bipolar events reveal how lightning is initiated in thunderstorms. *Nature communications*, *7*, 10721. doi: 10.1038/ncomms10721(2016)

Rubinstein, M., & Uman, M. A. (1990). On the radiation field turn-on term associated with traveling current discontinuities in lightning. *Journal of Geophysical Research: Atmospheres*, *95*(D4), 3711-3713. doi: 10.1029/JD095iD04p03711

Shao, X.-M., Fitzgerald, T. J., & Jacobson, A. R. (2005). Reply to comment by Rajeev Thottappillil and Vladimir A. Rakov on “Radio frequency radiation beam pattern of return strokes: A revisit to theoretical analysis”. *Journal of Geophysical Research: Atmospheres*, *110*(D24). doi: 10.1029/2005JD005889

Shao, X.-M., Jacobson, A. R., & Fitzgerald, T. J. (2004). Radio frequency radiation beam pattern of lightning return strokes: A revisit to theoretical analysis. *Journal of Geophysical Research: Atmospheres*, *109*(D19). doi: 10.1029/2004JD004612

Smith, D. A., Heavner, M. J., Jacobson, A. R., Shao, X. M., Massey, R. S., Sheldon, R. J., & Wiens, K. C. (2004). A method for determining intracloud lightning and ionospheric heights from VLF/LF electric field records. *Radio Science*, *39*(1), RS1010. doi: 10.1029/2002RS002790

Smith, D. A., Shao, X. M., Holden, D. N., Rhodes, C. T., Brook, M., Krehbiel, P. R., … Thomas, R. J. (1999). A distinct class of isolated intracloud lightning discharges and their associated radio emissions. *Journal of Geophysical Research: Atmospheres*, *104*(D4), 4189-4212. doi: 10.1029/1998JD200045

Thottappillil, R., & Rakov, V. (2001). On the computation of electric fields from a lightning discharge in time domain. In *2001 IEEE EMC international symposium on electromagnetic compatibility* (Vol. 2, pp. 1030–1035).

Thottappillil, R., & Rakov, V. A. (2005). Comment on “Radio frequency radiation beam pattern of lightning return strokes: A revisit to theoretical analysis” by Xuan-Min Shao, Abram R. Jacobson, and T. Joseph Fitzgerald, journal = Journal of Geophysical Research: Atmospheres. , *110*(D24). doi: 10.1029/2004JD005729

Thottappillil, R., Uman, M. A., & Rakov, V. A. (1998). Treatment of retardation effects in calculating the radiated electromagnetic fields from the lightning discharge. *Journal of Geophysical Research: Atmospheres*, *103*(D8), 9003-9013. doi: 10.1029/97JD02941

Tilles, J. N., Liu, N., Stanley, M. A., Krehbiel, P. R., Rison, W., Stock, M. G., … Wilson, J.

(2019). Fast negative breakdown in thunderstorms. *Nature communications*, *10*(1), 1648. doi: 10.1038/s41467-019-09621-z

Uman, M. A., & McLain, D. K. (1970). Radiation field and current of the lightning stepped leader. *Journal of Geophysical Research (1896-1977)*, *75*(6), 1058-1066. doi: 10.1029/JC075i006p01058

Uman, M. A., McLain, D. K., & Krider, E. P. (1975). The electromagnetic radiation from a finite antenna. *American Journal of Physics*, *43*(1), 33-38. doi: 10.1119/1.10027

Uman, M. A., Martin A., & McLain, D. K. (1970). Lightning return stroke current from magnetic and radiation field measurements. *Journal of Geophysical Research (1896-1977)*, *75*(27), 5143-5147. doi: 10.1029/JC075i027p05143

Watson, S. S., & Marshall, T. C. (2007). Current propagation model for a narrow bipolar pulse. *Geophysical Research Letters*, *34*(4). doi: 10.1029/2006GL027426

427 **Figure list**

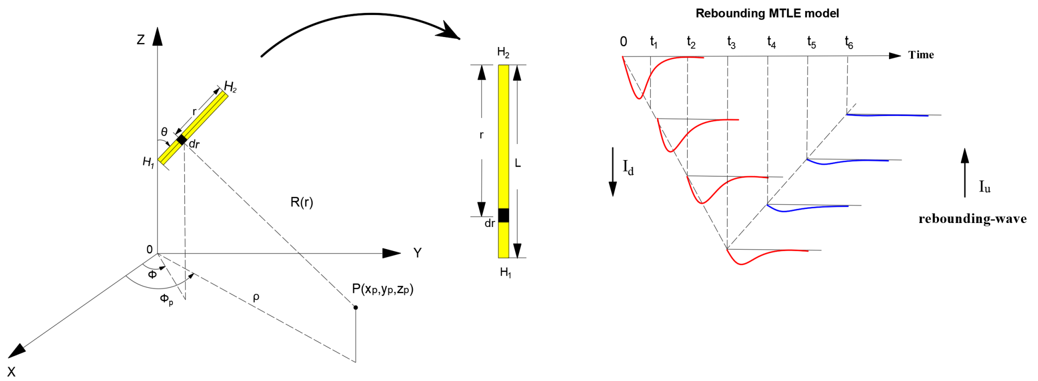

Figure 1. Geometry of the inclined NBE channel with a current that propagates following the rebounding MTLE model. (a) We model the NBE channel as a series of small straight segments at a radial distance of r and a polar angle θ with respect to the Z axis. The azimuth angle ϕ is defined by the angle between the X axis and the projection of the segment in the XY plane. The observation point $P(x_p, y_p, z_p)$ is at an altitude z_p above the ground surface and at a plane distance ρ from the source, thus $x_p = \rho\cos(\phi_p)$, $y_p = \rho\sin(\phi_p)$, where ϕ_p is the azimuth angle of the observation point P. (b) In the rebounding MTLE model, the NBE channel is considered as a system of positive streamer coronas that propagate downward from an altitude H_2 to H_1 with a channel length L, followed by upward negative streamer corona discharges that propagate back along the same path. Here, I_d is the downward current and I_u is the rebounding-wave current.

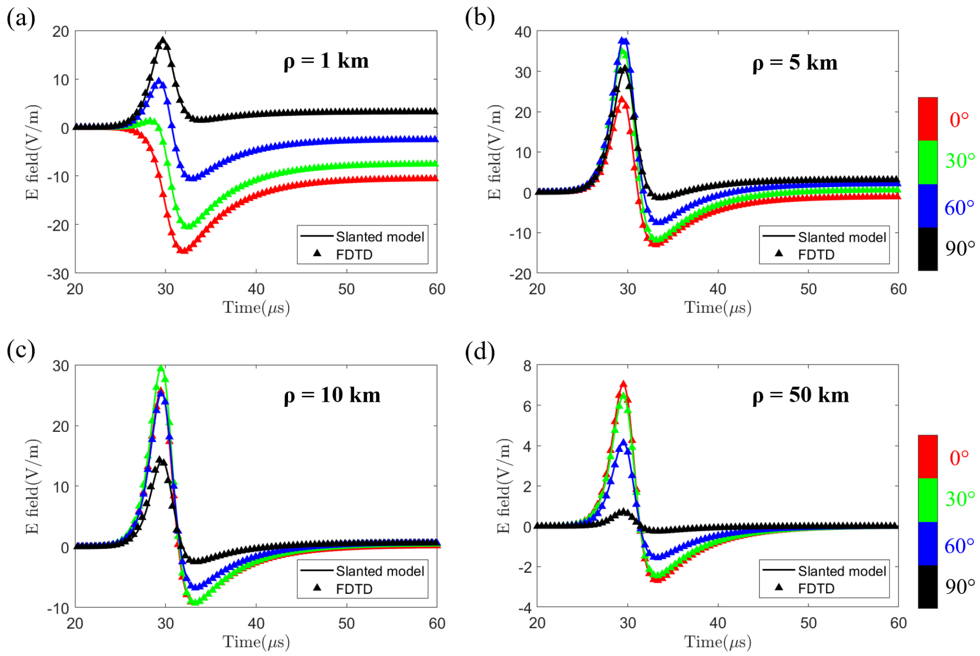

Figure 2. Comparison between the slanted rebounding wave model and FDTD method by considering the slanted dipole with different θ angles with respect to the z-axis and the azimuthal angle $\phi = 0°$ at a distance of 1 km, 5 km, 10 km and 50 km.

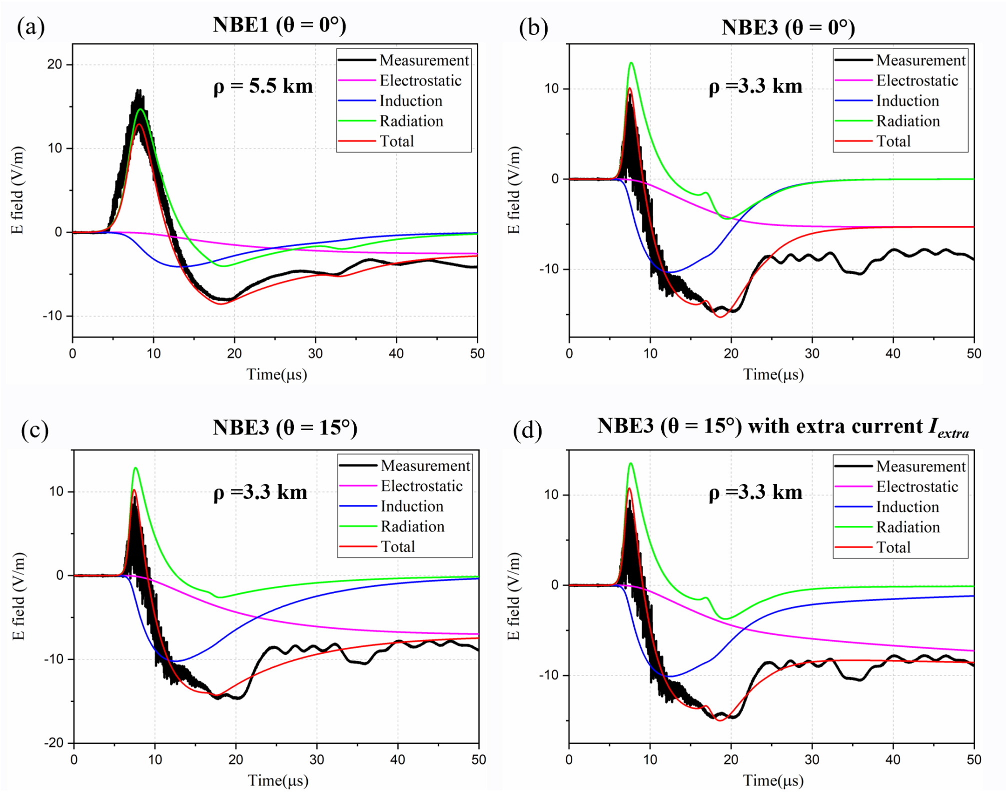

Figure 3. Comparison between the observations from Rison et al. (2016) and simulation results by assuming the vertical channel for NBE1(a) and NBE3(b) and the slanted channel for NBE3 without (c) and with (d) the extra current I_{extra}. The electrostatic, induction and radiation components of the total electric fields are also given in the figure.

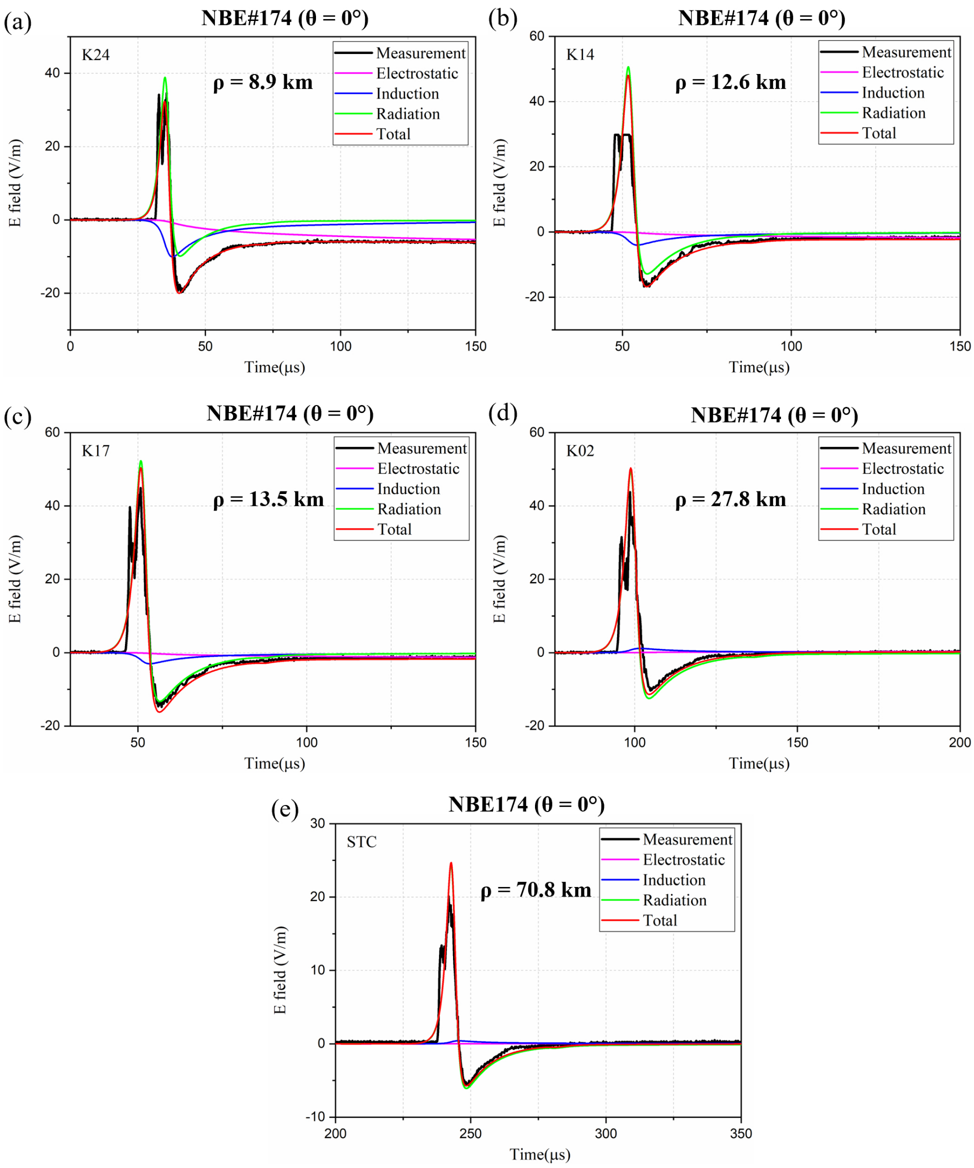

Figure 4. Comparison between the observations from Karunarathne et al. (2016) and simulation results by assuming a vertical channel for NBE#174 at different distances. The electrostatic, induction and radiation components of the total electric fields are also given in the figure.

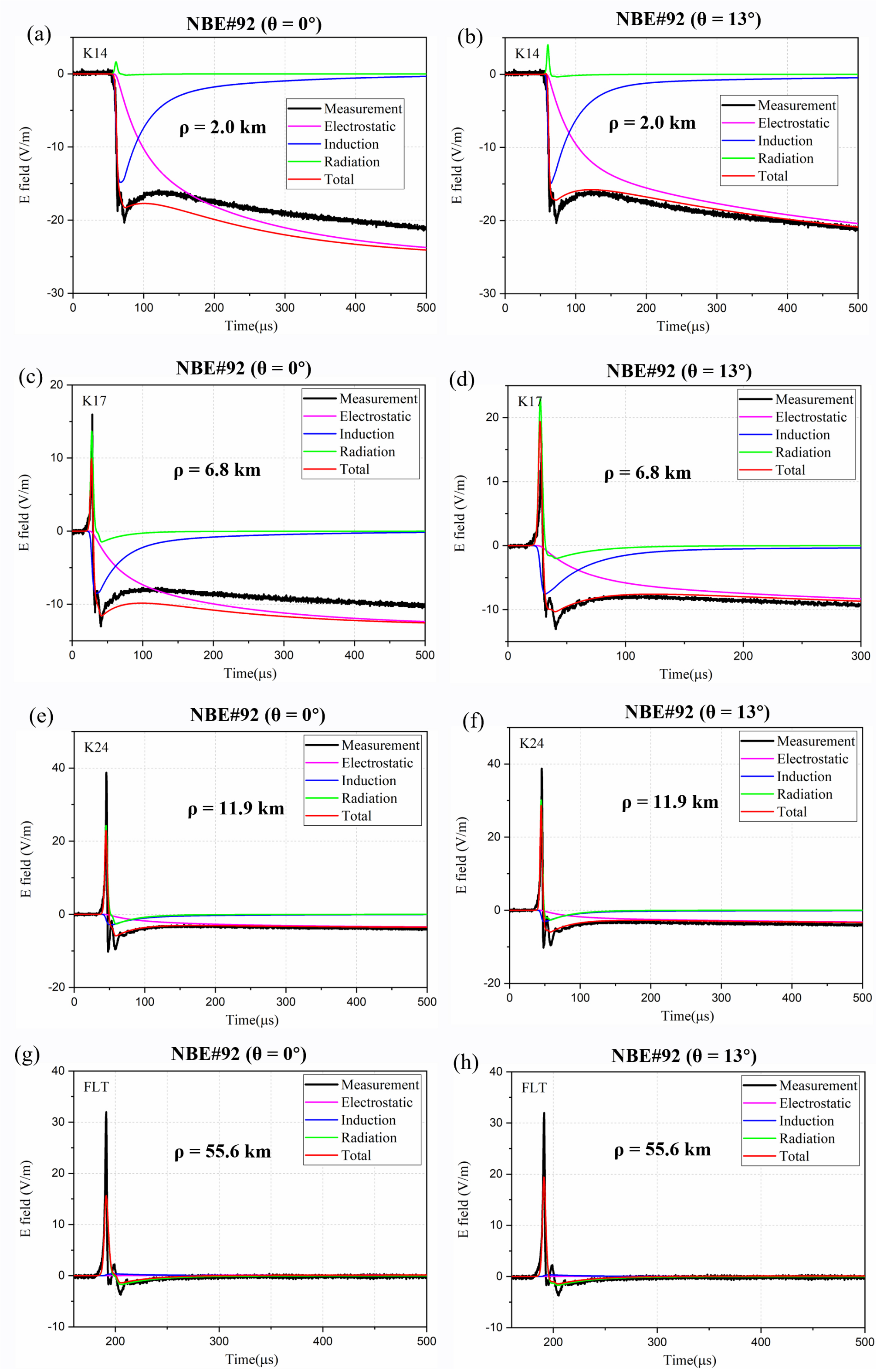

Figure 5. Comparison between the observations from Karunarathne et al. (2016) and simulation results by assuming a vertical channel (a,c,e,g) and a slanted channel (b,d,f,h) for NBE#92 at different distances. The electrostatic, induction and radiation components of the total electric fields are also given in the figure.

Supporting Information for "Propagation Effects of Slanted Narrow Bipolar Events: A Rebounding-Wave Model Study"

Dongshuai Li[1,2], Alejandro Luque[2], Farhad Rachidi[3], Marcos Rubinstein[4],

Torsten Neubert[1], Yanan Zhu[5], Olivier Chanrion[1], Caitano da Silva[6],

Paul R. Krehbiel[6]

[1]National Space Institute, Technical University of Denmark (DTU Space), Kongens Lyngby, Denmark.

[2]Instituto de Astrofísica de Andalucía (IAA), CSIC, Granada, Spain.

[3]Electromagnetic Compatibility Laboratory, Swiss Federal Institute of Technology (EPFL), Lausanne, Switzerland.

[4]University of Applied Sciences and Arts Western Switzerland, Yverdon-les-Bains, Switzerland.

[5]Earth Networks, Germantown, Maryland, USA.

[6]Langmuir Laboratory for Atmospheric Research, New Mexico Institute of Mining and Technology, Socorro, USA.

Contents of this file

Introduction This supplement contains additional information in support of the data and methods presented in the main text. **Text S1** describe the details of the discontinuity term related to the current discontinuity. **Figure S1** shows the side and top snapshot of the FDTD simulation for the vertical electric fields of the slanted dipole with $\theta = 0°$, $30°$, $60°$ and $90°$. **Figure S2** illustrates the electrostatic, induction and radiation components for both vertical and slanted dipoles at different distances. **Text S2** and **Figure S3** describe the transformation geometry of the slanted channel of NBE3. **Figure S4** shows the current distribution along the channel for the vertical NBE1, the vertical NBE3, and the slanted NBE3 without and with the extra current I_{extra}. **Figure S5** shows the current distribution along the channel for the vertical NBE#174 and the vertical NBE#92 and the slanted NBE#92. **Table S1** details the inferred features of the fast breakdowns corresponding to the NBEs reported from Rison et al. (2016); Karunarathne et al. (2016).

Text S1: The discontinuity term related to the current discontinuity

The so-called discontinuity term (Thottappillil et al., 1998; Thottappillil & Rakov, 2001),“turn-on” term (M. A. Uman & McLain, 1970; M. A. Uman Martin A. & McLain, 1970) or F factor (Rubinstein & Uman, 1990; Thottappillil & Rakov, 2001, 2005; Shao et al., 2004, 2005) should be considered if there is a current discontinuity at the propagation wave front. Note that the discontinuity term is only applicable if there is a current discontinuity (Thottappillil et al., 1998; Thottappillil & Rakov, 2001). The discontinuity term and its image are given by

$$dE_{zc}^{disc} = \frac{dL'}{4\pi\epsilon_0}\left(\begin{array}{c} \frac{(z_p-(L'\cos\theta+H_1))(x_p-L'\sin\theta\cos\phi)}{c^2R^3(L')}\sin\theta\cos\phi \\ +\frac{(z_p-(L'\cos\theta+H_1))(y_p-L'\sin\theta\sin\phi)}{c^2R^3(L')}\sin\theta\sin\phi \\ -\frac{(z_p-(L'\cos\theta+H_1))^2-R^2(L')}{c^2R^3(L')}\cos\theta \end{array}\right) I(L', t-R(L')/c-(H_2-r)/v)\frac{dL'}{dt}, \quad (1)$$

and its image,

$$dE_{zm}^{disc} = -\frac{dL'}{4\pi\epsilon_0}\left(\begin{array}{c} \frac{(z_p+(L'\cos\theta+H_1))(x_p-L'\sin\theta\cos\phi)}{c^2R_0^3(L')}\sin\theta\cos\phi \\ +\frac{(z_p+(L'\cos\theta+H_1))(y_p-L'\sin\theta\sin\phi)}{c^2R_0^3(L')}\sin\theta\sin\phi \\ -\frac{(z_p+(L'\cos\theta+H_1))^2-R_0^2(L')}{c^2R_0^3(L')}\cos\theta \end{array}\right) I(L', t-R_0(L')/c-(H_2-r)/v)\frac{dL'}{dt}, \quad (2)$$

where L' and $\frac{dL'}{dt}$ are, respectively, the retarded channel length and the speed of the current wave front as seen by the observer at P. v is the propagation velocity. $\frac{dL'}{dt}$ can be expressed as Rubinstein & Uman (1990); Thottappillil & Rakov (2001, 2005); Shao et al. (2004, 2005),

$$\frac{dL'}{dt} = \frac{v}{1-(v/c)\cos(\alpha(L'))} = vF(L'), \quad (3)$$

where $\alpha(L')$ is the angle between the direction of propagation and the line connecting the retarded position of the wave front and the observation point at P. The F factor is

$$F(L') = \frac{1}{1-(v/c)\cos(\alpha(L'))}. \quad (4)$$

Text S2: The transformation geometry of the slanted channel of NBE3

As shown in Figure S3(a), we assume the plane containing the NBE channel is perpendicular to the transfer vector $T = (x'_1, y'_1, 0)$ (see the red vector) with a distance ρ from the observation point P' is at the origin (0, 0, 0). The injection point $R'_1 = (x'_1, y'_1, z'_1)$ and end point $R'_2 = (x'_2, y'_2, z'_2)$ of the NBE channel are at radial distances of r_1 and r_2 away from the observer, respectively, with the elevation angle θ'_{el} ranging from 62° to 63.5° and azimuth angle ϕ'_{az} ranging from 338° to 340° (see Figure 9 in the Supplementary Material of Rison et al. (2016)). Assuming the NBE current propagates downward, the direction vectors for R'_1 and R'_2 can be written as

$$\begin{aligned} \vec{u_1} &= (\sin\theta'_1 \cos\phi'_1,\ \sin\theta'_1 \sin\phi'_1,\ \cos\theta'_1), \\ \vec{u_2} &= (\sin\theta'_2 \cos\phi'_2,\ \sin\theta'_2 \sin\phi'_2,\ \cos\theta'_2), \end{aligned} \tag{5}$$

where the polar angle $\theta' = 90° - \theta'_{el}$ and azimuthal angle $\phi' = \phi'_{az}$. The injection point R'_1 and the end point R'_2 can be calculated as

$$\begin{aligned} R'_1 &= r_1 \vec{u_1}, \\ R'_2 &= r_2 \vec{u_2}, \end{aligned} \tag{6}$$

where the radial distance $r = \rho / \cos(\theta'_{el})$, $\rho = 3.3\,\mathrm{km}$ is the length of the transfer vector T corresponding to the plane distance between the source and the observer (Rison et al., 2016).

Once R'_1 and R'_2 have been obtained, we focus on the transformation from the geometry shown in Figure S3(a) (named as A') to the geometry given by Figure S3(b) (named as A). The relationship between two different geometries is then written

$$A' = T + A, \tag{7}$$

where the transfer vector $T = (x'_1, y'_1, 0)$ by moving the injection point R'_1 of the NBE channel back to the Z axis. Finally, based on geometry A in Figure S3(b), the new end point $R_2 = R'_2 - T = (x'_2 - x'_1, y'_2 - y'_1, 0)$ and the new observation point $P = P' - T = (-x'_1, -y'_1, 0)$. The new azimuthal angle of the source ϕ and the new azimuthal angle of the observer ϕ_p, defined counterclockwise from the positive x-axis (North direction), can be calculated as:

$$\begin{aligned} \phi &= 270^\circ - \arctan\left(\frac{|x'_2 - x'_1|}{|y'_2 - y'_1|}\right) = 249^\circ, \\ \phi_p &= 90 + \arctan\left(\frac{|-x'_1|}{|-y'_1|}\right) = 160^\circ. \end{aligned} \tag{8}$$

Table S1

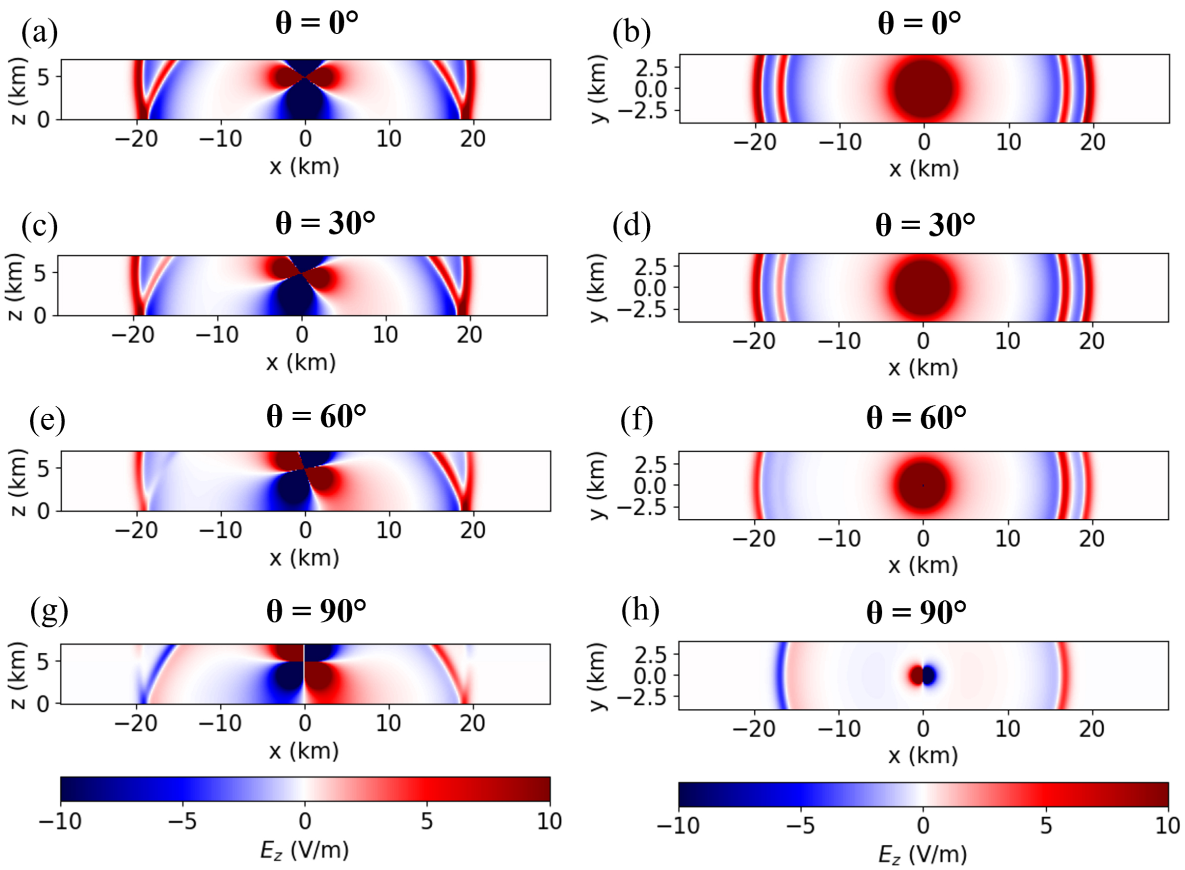

Figure S1. Side (a,c,e,g) and top (b,d,f,h) view of a snapshot of the FDTD simulation for the vertical electric fields of the slanted dipole with the polar angle $\theta = 0°$(vertical dipole), 30°, 60°and 90°(horizontal dipole).

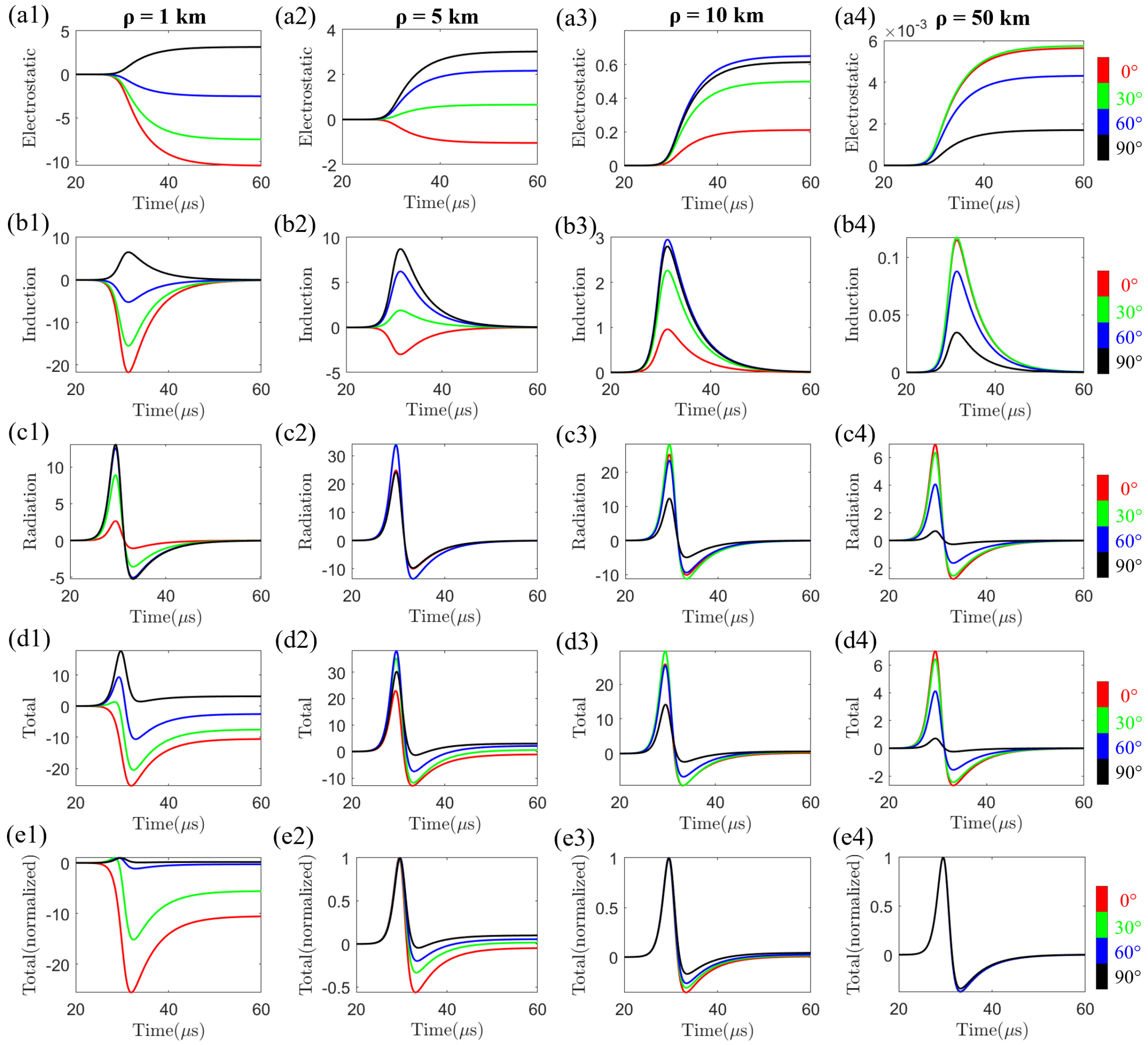

Figure S2. Electrostatic (a1-a4), Induction (b1-b4), and Radiation (c1-c4) components of the total electric fields (d1-d4) and the normalized total electric fields (e1-e4) for the slanted dipole with different θ angles with respect to Z axis and the azimuthal angle $\phi = 0°$ at a distance of 1 km, 5 km, 10 km and 50 km.

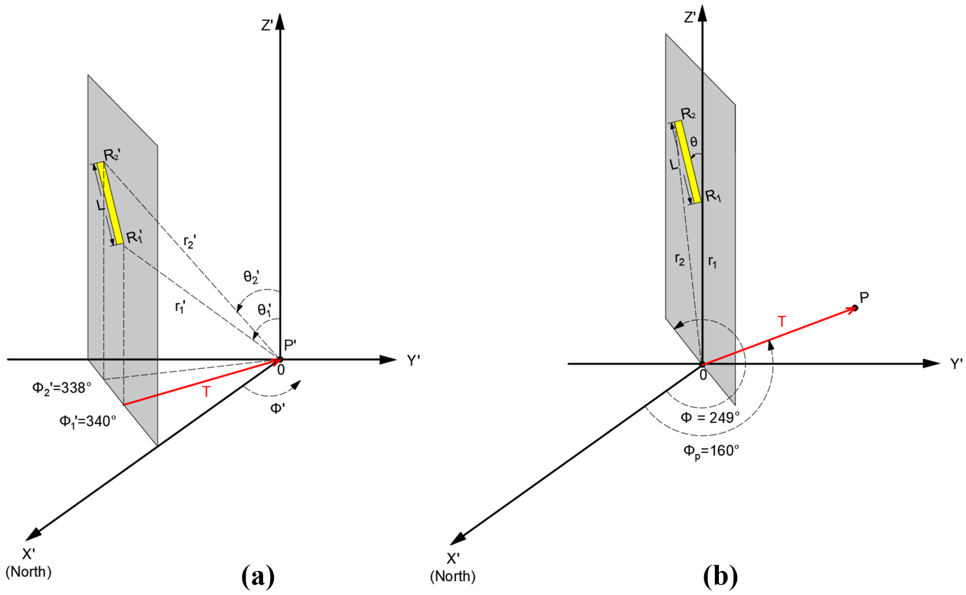

Figure S3. Schematic procedure to obtain the geometry of the slanted channel of NBE3. The transfer vector $T = (x'_1, y'_1, 0)$ from geometry A'(a) to A(b) is marked by the red arrow. (a) The geometry of the interferometer in Rison et al. (2016) (defined as A') with the observation point P' at the origin and the injection point R'_1 and the end point R'_2 of the NBE channel located at a plane that is perpendicular to the transfer vector T with a distance ρ. The azimuth angles for the channel ends range from $\phi'_2 = 338°$ to $\phi'_1 = 340°$ and (b) the geometry adopted in our study (defined as A) with the injection point R_1 of the NBE channel located on the Z axis and the observation point P located at T with a distance ρ and an azimuth angle $\phi_p = 160°$.

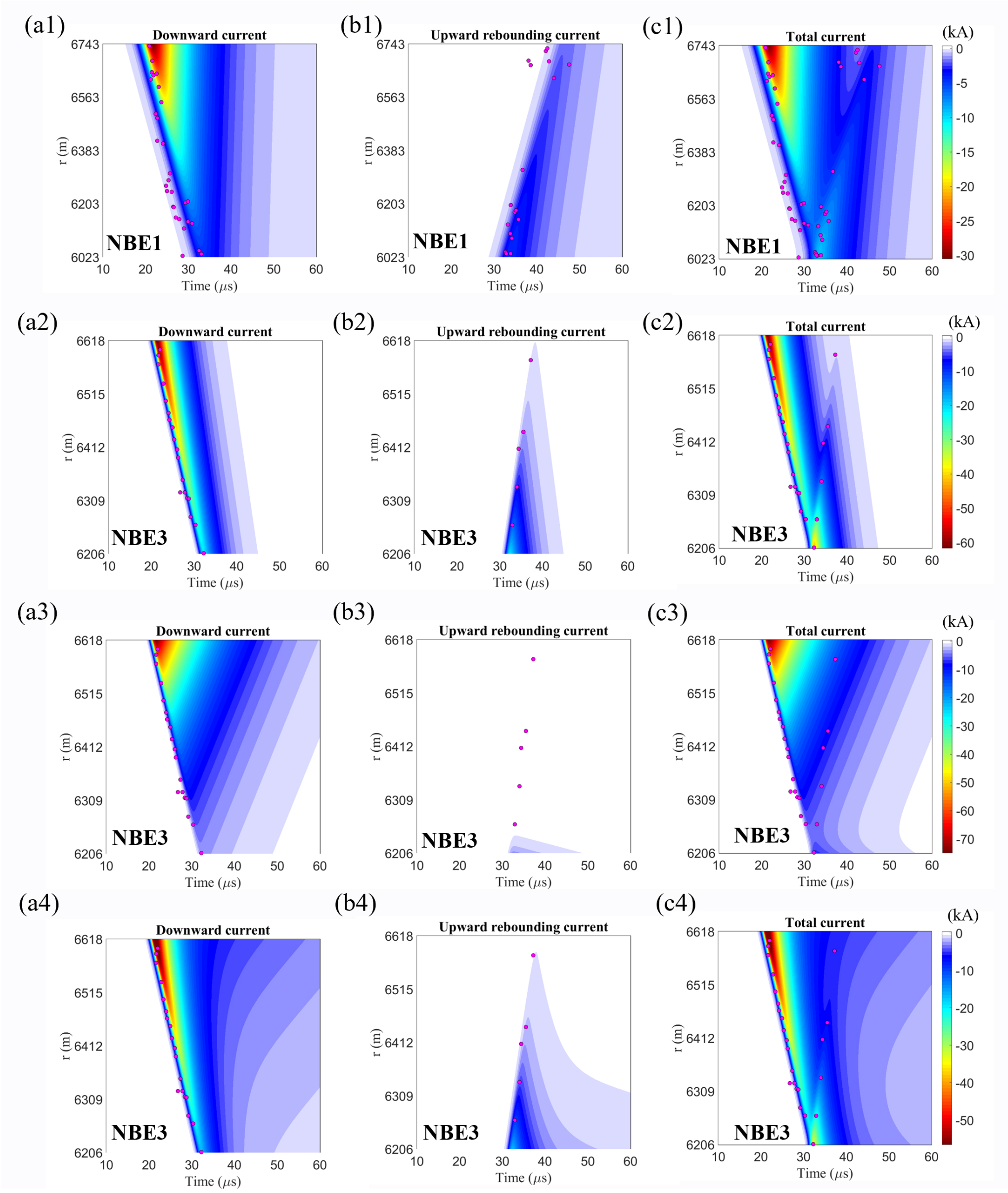

Figure S4. The downward, upward and total current distribution based on the rebounding MTLE model for the vertical NBE1(a1,b1,c1) and the vertical NBE3(a2,b2,c2), the slanted NBE3 without the extra current I_{extra}(a3,b3,c3) and the slanted NBE3 with the extra current I_{extra} (a4,b4,c4). The INTF data corresponding to the source time are marked by the pink dots.

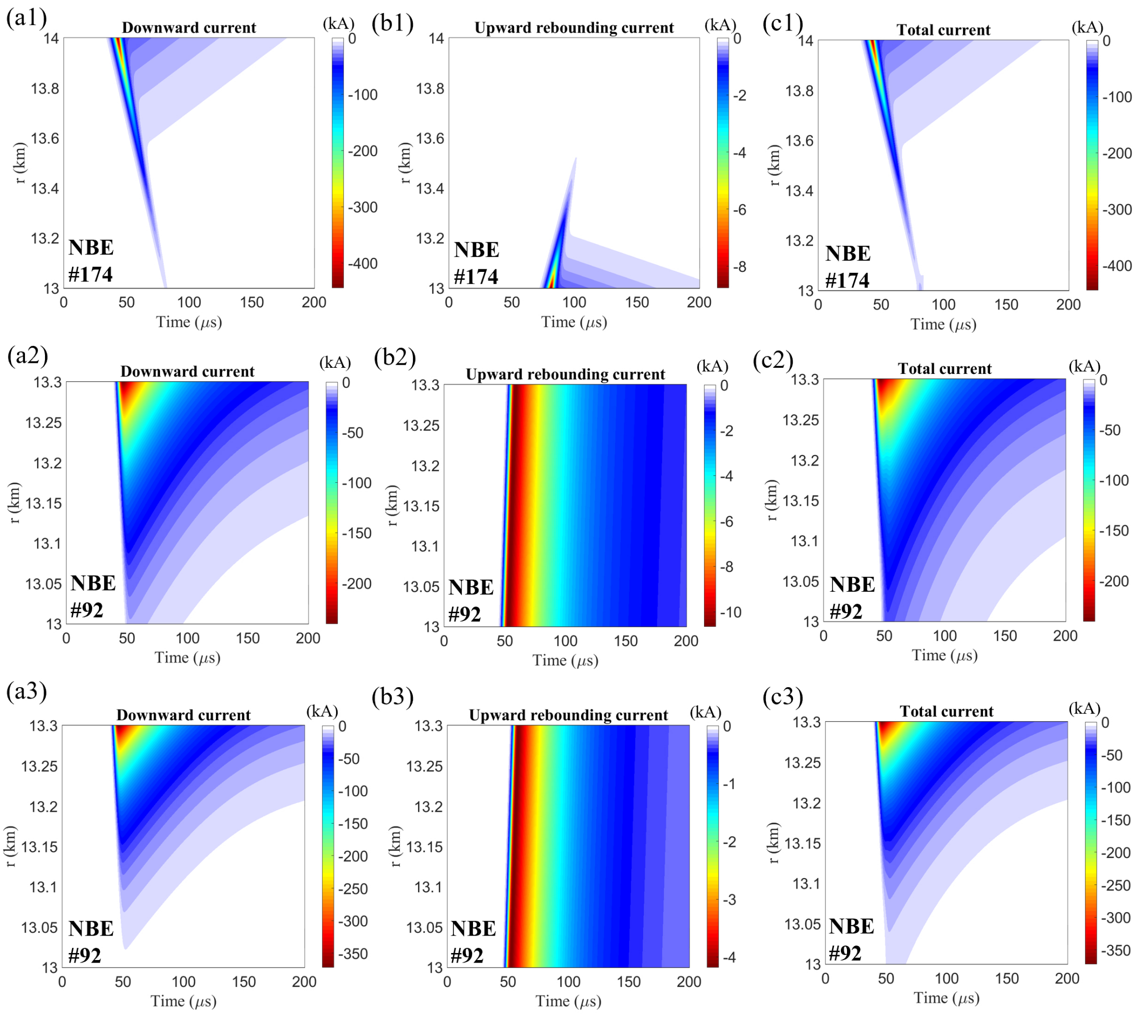

Figure S5. The downward, upward and total current distribution based on the rebounding MTLE model for the vertical NBE#174(a1,b1,c1) and the vertical NBE#92(a2,b2,c2) and the slanted NBE#92(a3,b3,c3) in Karunarathne et al. (2016).

Table S1. The inferred features of the fast breakdowns corresponding to the vertical NBE1, the vertical NBE3 , the slanted NBE3 without and with the extra current I_{extra}, the vertical NBE#174, the vertical NBE#92, and the slanted NBE#92.

ID	Inclination	Polar angle	Simulation-determined parameters								INTF-determined parameters				
		θ	I_{peak} (kA)	τ_1 (μs)	τ_2 (μs)	I_{peak}^{extra} (kA)	τ_3 (μs)	λ_d (m)	λ_u (m)	Q_{mom} (C·m)	ρ (km)	H_2 (km)	L (m)	t_d* (μs)	t_u* (μs)
NBE1	Vertical	0°	-30.5	0.8	7.0	-	-	374.9	857.6	-215	5.5	6.7	720	12	13
NBE3	Vertical	0°	-61.7	0.3	3.4	-	-	378.7	113.7	-116	3.3	6.6	412	11	6
	Slanted	15°	-75	0.3	10.4	-	-	136.6	22.1	-357	3.3	6.6	412	11	6
	Slanted	15°	-56.6	0.3	3.2	-7.4	39.7	305.4	98.3	-219	3.3	6.6	412	11	6

ID	Inclination	Polar angle	Simulation-determined parameters								Other parameters		
		θ	I_{peak} (kA)	τ_1 (μs)	τ_2 (μs)	I_{peak}^{extra} (kA)	τ_3 (μs)	λ_d (m)	λ_u (m)	Q_{mom} (C·m)	H_2 (km)	L† (m)	v† (m/s)
NBE#174	Vertical	0°	-426.5	2.0	1.2	-34.9	78.1	257.3	125.8	-4775	13	1000	2.6×10^7
NBE#92	Vertical	0°	-200.6	1.0	31.4	-41.0	196.0	96.2	1×10^5	-4519	13.3	300	5×10^7
	Slanted	13°	-345.2	0.9	32.6	-28.9	410.1	66.8	1×10^5	-6958	13.3	300	5×10^7

* The downward and upward propagation time t_d and t_u are determined by fitting the INTF traces for both NBE1 and NBE3 in Rison et al. (2016).

† The channel length L and the propagation velocity v are obtained from Karunarathne et al. (2016); Rison et al. (2016).

References

Karunarathne, S., Marshall, T. C., Stolzenburg, M., & Karunarathna, N. (2016). Electrostatic field changes and durations of narrow bipolar events. *Journal of Geophysical Research: Atmospheres*, *121*(17), 10,161-10,174. doi: https://doi.org/10.1002/2016JD024789

Rison, W., Krehbiel, P. R., Stock, M. G., Edens, H. E., Shao, X.-M., Thomas, R. J., … Zhang, Y. (2016). Observations of narrow bipolar events reveal how lightning is initiated in thunderstorms. *Nature communications*, *7*, 10721. doi: 10.1038/ncomms10721(2016)

Rubinstein, M., & Uman, M. A. (1990). On the radiation field turn-on term associated with traveling current discontinuities in lightning. *Journal of Geophysical Research: Atmospheres*, *95*(D4), 3711-3713. doi: 10.1029/JD095iD04p03711

Shao, X.-M., Fitzgerald, T. J., & Jacobson, A. R. (2005). Reply to comment by Rajeev Thottappillil and Vladimir A. Rakov on "Radio frequency radiation beam pattern of return strokes: A revisit to theoretical analysis". *Journal of Geophysical Research: Atmospheres*, *110*(D24). doi: 10.1029/2005JD005889

Shao, X.-M., Jacobson, A. R., & Fitzgerald, T. J. (2004). Radio frequency radiation beam pattern of lightning return strokes: A revisit to theoretical analysis. *Journal of Geophysical Research: Atmospheres*, *109*(D19). doi: 10.1029/2004JD004612

Thottappillil, R., & Rakov, V. (2001). On the computation of electric fields from a lightning discharge in time domain. In *2001 IEEE EMC international symposium on electromagnetic compatibility* (Vol. 2, pp. 1030–1035).

Thottappillil, R., & Rakov, V. A. (2005). Comment on "Radio frequency radiation beam pattern of lightning return strokes: A revisit to theoretical analysis" by Xuan-Min Shao, Abram R. Jacobson, and T. Joseph Fitzgerald, journal = Journal of Geophysical Research: Atmospheres. , *110*(D24). doi: 10.1029/2004JD005729

Thottappillil, R., Uman, M. A., & Rakov, V. A. (1998). Treatment of retardation effects in calculating the radiated electromagnetic fields from the lightning discharge. *Journal of Geophysical Research: Atmospheres*, *103*(D8), 9003-9013. doi: 10.1029/97JD02941

Uman, M. A., & McLain, D. K. (1970). Radiation field and current of the lightning stepped leader. *Journal of Geophysical Research (1896-1977)*, *75*(6), 1058-1066. doi: 10.1029/JC075i006p01058

Uman, M. A., Martin A., & McLain, D. K. (1970). Lightning return stroke current from magnetic and radiation field measurements. *Journal of Geophysical Research (1896-1977)*, *75*(27), 5143-5147. doi: 10.1029/JC075i027p05143